ISSN: 3069-5538

Research Article

Current Research in Traffic Transportation Engineering

Internally Generated Voltage Signals in Self-Oscillating Casimir–Electrostatic Mems with Conserved Energy Dynamics

Patrick Sangouard*

Retired from E.S.I.E.E : Ecole Supérieure Ingénieurs Electronique Electrotechnique, Paris, France

***Corresponding Author**
Patrick Sangouard, Retired from E.S.I.E.E: Ecole Supérieure Ingénieurs Electronique Electrotechnique, Paris, France.
Email: sangouard2.patrick@gmail.com

Submitted: 2026, Apr 20; **Accepted:** 2026, May 25; **Published:** 2026, Jun 08

Citation: Sangouard, P. (2026). Internally Generated Voltage Signals in Self-Oscillating Casimir–Electrostatic Mems with Conserved Energy Dynamics. *Curr Res Traffic Transport Eng, 4*(1), 01-33.

Abstract

We present a theoretical model of a Casimir-effect micro/nano-electromechanical system exhibiting self-oscillating behavior and internally generated voltage signals, strictly within the framework of Emmy Noether's theorem. The device consists of a fixed piezoelectric beam mechanically coupled to a movable electrode subjected to Casimir attraction at nanometer distances. The mechanical deformation of the beam induces piezoelectric charges that drive a synchronized electrostatic switching sequence. This sequence involves complementary MOS switches connected to a Coulomb electrode and a passive RLC circuit. The operating principle relies on a redistribution of electrical charges induced by the deformation, transiently generating electrostatic forces that oppose Casimir attraction. This controlled force imbalance induces rapid mechanical relaxation, leading to a stable self-oscillating cycle.

Coupled electromechanical simulations, performed with MATLAB, ANSYS, and SPICE, show that, for realistic material parameters and device geometries, the system supports nanometer-amplitude oscillations at characteristic frequencies on the order of MHz, generating internal voltage signals across the circuit. It is important to note that the model does not predict any net energy extraction from the quantum vacuum. The Casimir interaction is treated as a conservative boundary force, and the observed dynamics result from an internal redistribution of mechanical and electrostatic energy, with dissipative losses explicitly accounted for. Any voltage signal generated by the device is strictly limited by the mechanical work performed during each oscillation cycle.

In addition to the dynamic model, this work describes an original device architecture that integrates oscillatory peak signals converted into a self-sustaining DC voltage of several volts via a power-less electronic module, stored on a capacitive electronic system. A fabrication strategy compatible with standard SOI processes allows for control of nanometric spaces without resorting to extreme lithography. The proposed framework offers a testable platform for exploring Casimir-assisted electromechanical dynamics in energy-efficient MEMS and invites critical experimental and theoretical evaluation.

Keywords: Casimir, Coulomb, Quantum vacuum fluctuations, Piezoelectric, MEMS, NEMS

1. Description of the System

1.1. Introduction

As micro- and nano-electromechanical systems (MEMS/NEMS) approach nanometric dimensions, surface-dominated interactions increasingly govern their mechanical and electrical behavior. Among these interactions, the Casimir force—arising from modifications of the quantum electromagnetic vacuum induced by boundary conditions—becomes significant at sub-micrometric separations and has been experimentally confirmed with high precision. Although the Casimir interaction originates from quantum vacuum fluctuations,

it can be treated, for practical device modeling, as a conservative force whose magnitude depends solely on geometry and material properties.

In recent years, Casimir-assisted dynamics have been investigated in the context of actuation, sensing, and stability control in nanoscale systems. When combined with elastic structures and electromechanical transduction mechanisms, the strong distance dependence of the Casimir force enables nontrivial couplings between mechanical motion and electrical degrees of freedom. Importantly, such couplings do not imply the existence of an exploitable energy reservoir in the vacuum; rather, they reflect a redistribution of energy within a closed system whose total energy remains conserved.

In this work, we propose and analyze a theoretical Casimir–electrostatic MEMS architecture that exhibits self-oscillating behavior and internally generated voltage signals within a strictly energy-conserving framework. The device couples Casimir-induced mechanical motion to piezoelectric charge generation and synchronized electrostatic switching, leading to a cyclic exchange between mechanical, electrical, and elastic energy components.

All contributions, including mechanical deformation, electrical charge transport, and dissipative losses, are described within a single Hamiltonian framework in which the Casimir interaction enters as a geometry-dependent vacuum energy term. The analysis explicitly respects the conditions required by Emmy Noether's theorem: the invariance of the system under time translations ensures global energy conservation throughout the oscillatory cycle. The quantum vacuum is therefore not treated as an independent dynamical reservoir, but as a conservative contribution to the total energy of the coupled electromechanical system. Within this description, the observed oscillatory dynamics arise from internal energy redistribution rather than from any net extraction of energy from the vacuum.

Beyond the dynamical model, the proposed architecture incorporates an original integration of switching electronics and a fabrication strategy compatible with standard silicon-on-insulator (SOI) processes, enabling controlled nanometric gaps without resorting to extreme lithography. The present work is purely theoretical and aims to provide a coherent and testable framework for exploring Casimir-assisted electromechanical dynamics in energy-conserving MEMS, while inviting critical experimental and theoretical evaluation of the underlying assumptions and predicted behavior. The Casimir interaction is a well-established consequence of quantum field boundary conditions and does not constitute an energy source; however, its influence on the dynamics and stability of micro- and nano-electromechanical systems remains an active area of investigation.

We explore a model where a piezoelectric bridge is deformed by an isotropic, atemporal, attractive Casimir force F_{CA}, and restored by a transient, repulsive Coulomb force F_{CO} induced by the deformation. The schematic of this MEMS is shown in Figures 1 and 2.

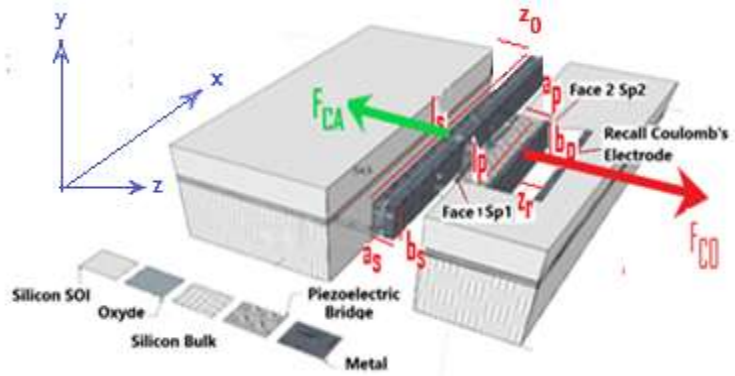

Figure 1: Vue of the Top of Device, Axes, Forces , Casimir's Electrodes Piezoelectric Bridge Recall Coulomb's Electrode *a_p, b_p and l_p , are Thickness, Width, and Length of the Piezoelectric Bridge
*a_p, b_p and l_p , are thickness, width, and length of the piezoelectric bridge.
*a_s, b_s and l_s , are the thickness, width and length of the Casimir moving electrode .

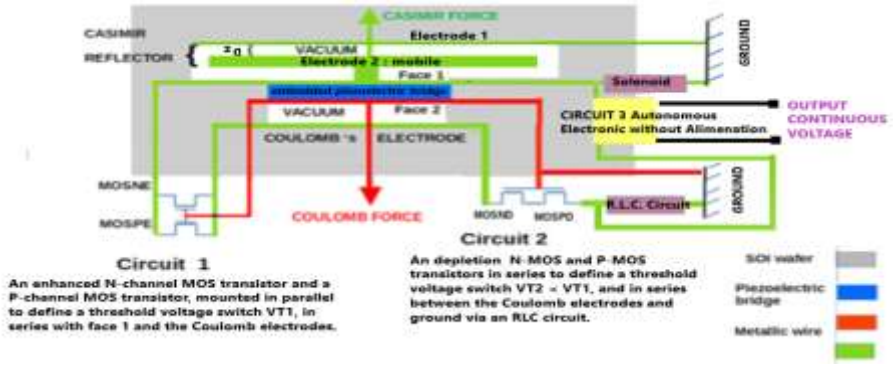

Figure 2: General Configuration of the Device: MOS Grid Connections (Face 2 of the Piezoelectric Bridge: Red), Source Connections (Face 1 of the Piezoelectric Bridge: Green)

The challenge lies in analyzing energy interactions without introducing net losses or gains that violate conservation principles (Emmy Noether theorem) . The attractive Casimir force is given by $F_{CA} = S_S \frac{\pi^2 \hbar c}{240 z_s^4}$ (Eq. 1), where $S_s = l_s b_s$ is the surface area of the Casimir electrodes, $\hbar = h/2\pi$ is the reduced Planck constant, c is the speed of light, and z sis the time gap dependent between Casimir electrodes [1,2,3]. The initial gap being z_0. This force varies as $1/z_s^4$, suggesting that a stronger opposing force could be needed at smaller gaps.

Fixed charges Q_F induced by the Casimir force in a piezoelectric film (perpendicular to polarization) are proportional to F_{CA}, thus varying as $1/z_s^4$: $Q_F = \frac{d_{31} l_p}{a_p} F_{CA} \Rightarrow Q_F = \frac{d_{31} l_p}{a_p} S_S \frac{\pi^2 \hbar c}{240} \left(\frac{1}{z_s^4} - \frac{1}{z_0^4} \right)$ (Eq. 2), [4,5,6] where z_0 is the initial gap without deformation, d_{31}(C/N) is the piezoelectric coefficient, and l_p, a_p are the length and thickness (m) of the piezoelectric bridge. The electric charge Q_F is independent of the common width $b_p = b_s = b_i$ (Figures 1,2,3), simplifying fabrication. It should be noted that Q_F equals zero when z_S is equal to z_0, meaning the piezoelectric bridge does not undergo any deformation.

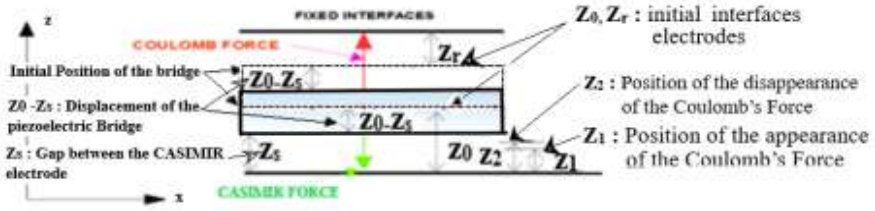

Figure 3: Cycle Diagram Showing Deformation and Return Phases With Forces and Positions

These fixed electric and ionic charges in the piezoelectric bridge have opposite signs and induce an electric field that attracts – from the mass- mobile charges of opposite signs to the metallized faces.

The mobile charges on face 2 (Figures 1,2) activate the insulating gates of enriched Thin Film Transistor Metal Oxide Semiconductor (TFT MOS) N and P [11], in parallel for switch №1 (Figure 4).

This generates a gate voltage $V_g = \frac{Q_F}{C_{ox}}$ (Eq. 3), where $C_{ox} = \frac{\epsilon_0 \epsilon_{ox}}{t_{ox}} L_T W_T$ (Eq. 4), (fig. 1,2), with ϵ_0 the vacuum permittivity, ϵ_{ox} the relative permittivity of silicon oxide, and L_T, W_T, t_{ox} the gate length, width, and thickness of the TFT MOS. The mobile charges on face 1 supply the sources of the TFT MOS N and P in parallel of switch №°1, allowing these electrics charges to homogenize with a Coulomb electrode if the threshold voltage of switch №1 is exceeded (Figure 4,5).

The Coulomb force exerted across the electrode interval $z_r + z_0$ - zs, in association with the electric charges Q_F, exhibits a variation proportional to $1/z_s^{10}$ (see Eq. 5 and Fig. 3). This force may counterbalance the Casimir force and contribute to equilibrium within the system, thereby facilitating a stable energy cycle in accordance with Noether's theorem. Note that prior to closing switch №1, the Coulomb electrode is automatically grounded via switch №2, composed of depletion-mode N and P MOS TFTs in series (Figure 1,2,4,6).

Key Notes:: This MEMS includes two automatic switches №1; №2 triggered by a threshold difference of some ten's millivolts of difference (Figure 4).

• Threshold voltages are V_{T1} for switch №1 and V_{T2} for switch №2, with | V_{T1} | slightly above | V_{T2} | by some tens of millivolts.
• If the gate voltage exceeds the threshold, switch №1 turns ON , while switch №2 turns OFF (Figure 4,5,6).

1.2. Description of Switches №1 and №2 and Self-contained Passive Switching and Rectification Circuitry

1.2.1 Switches Electronic Description

These automatic switches are fabricated using:
• Circuit №1 (Figure 5): Enriched TFT MOS P and MOS N in parallel, with thresholds V_{TPE} and V_{TNE} , call V_{T1}.
• Circuit №2 (Figure 6): Depletion TFT MOS P and MOS N in series, with thresholds V_{TPD} and V_{TND} , call V_{T2}.

Threshold voltages are arranged as: $V_{TPE} < V_{TND} < 0 < V_{TPD} < V_{TNE}$. For symmetry, $|V_{TPE}| \approx |V_{TNE}|$ and $|V_{TPD}| \approx |V_{TND}|$. Thus, $|V_{T2}| < |V_{T1}|$ minus only ten millivolts. So, switches №1 and №2 function at slightly different voltage levels, resulting in variations in their operating times (see Figures 1–6).

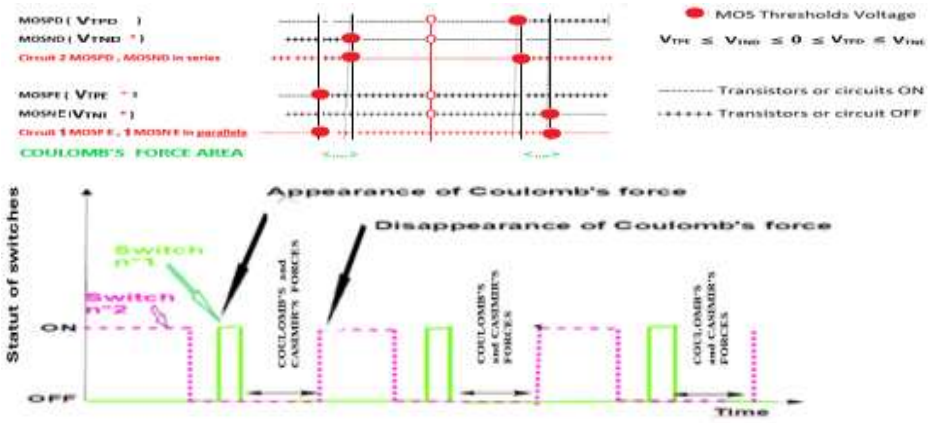

Figure 4: Distribution of Threshold Voltages of Enriched and Depleted N and P MOS Switches and Timing of These Switches

If $V_G > V_{T1}$, switch № 1 is ON , but if $V_G > V_{T2}$, switch № 2 is OFF . Switch №2 therefore opens very slightly before switch №1 closes. Similarly, switch №2 closes slightly switch after switch №1 opens.

Consequently, both switches № 1 and №2 are closed together for a short period (Figure 4). It is during this period that the Coulomb force on the piezoelectric bridge exerts a strong force opposing the Casimir force. When switch № 2 is closed, the Coulomb electrode is grounded through the RLC circuit, thereby neutralizing the Coulomb force.

1.2.2 Circuit №1: Switch №1

Switch №1 consists of enriched N-type TFT MOS (threshold V_{TNE}) in parallel with enriched P-type TFT MOS (threshold V_{TPE}) (Figures 5,6), positioned as in Figure 5 [11].

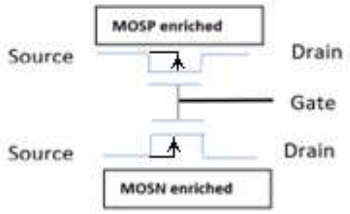

Circuit №1 - Switch №1 with enriched TFT MOS P and N in parallel.

Figure 5: Switch №1

Common gates are controlled by free charges on face №2 of the piezoelectric bridge. Sources are connected to face №1, drains to the Coulomb electrode (Figures 2,4,5).

Two types of Enriched MOS (type PE or NE) are used in parallel to handle either holes or electrons on face №1. Preferably and for

reason, of symmetry , $|V_{TNE}| \approx |V_{TPE}|$. The RLC circuit input is in series between the return Coulomb electrode and ground, with self-contained passive switching and rectification circuitry №3 in parallel (Figures 1,2,30). The return Coulomb electrode is grounded via switch №2.

1.2.3 Circuit №2: Switch №2

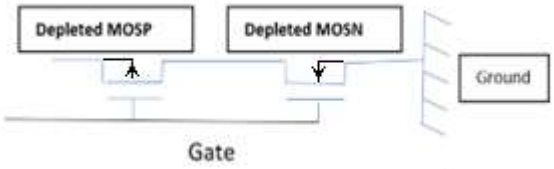

Circuit №2 - Switch №2 with depleted TFT MOS P and N in series

Figure 6: Switch №2

Switch №2 consists of depletion P-type TFT MOSPD in series with N-type MOSND (Figures 2,4,6). Common gates are controlled by free charges on face №2 (Figures 1,4,5). Input connects to the Coulomb electrode, output to the RLC circuit and ground. Preferably, $|V_{TND}| = |V_{TPD}|$, with values lower but close (less than 10%) to $|V_{TNE}| \approx |V_{TPE}|$.

1.3. Schematic and Behavior of the MEMS

When effective (switch №1 closed), the Coulomb return force F_{CO} is (Figures 1,2,3,4):

$$F_{CO} = \frac{Q_p^2}{4\pi\epsilon_0\epsilon_r}\left(\frac{1}{z_r+z_0-z_s}\right)^2 = \left[\frac{d_{31}l_p}{a_p}S_s\frac{\pi^2\hbar c}{240}\left(\frac{1}{z_s^4}-\frac{1}{z_0^4}\right)\right]^2\left(\frac{1}{8\pi\epsilon_0\epsilon_r}\right)\left(\frac{1}{z_r+z_0-z_s}\right)^2 \text{(Eq. 5)}$$

Note that F_{CO} varies as $1/z_s{}^{10}$, with z_s the time-dependent gap and z_0 the initial gap. The sensor part schematic is in Figures 1 and 2.

The isotropic and timeless Casimir force, arising from quantum vacuum fluctuations, deforms into a microscopic piezoelectric bridge that is embedded in a silicon wafer (see figures 1 and 2). When switch №1 is open, mobile charges on face №1 remain there (fig 1,2) . Because an electric field can't exist in a perfect conductor, when switch №1 is closed and switch №2 is open, the electric charges must equalize between face №1 and the Coulomb electrode. If these two electrodes are equal, then charge on the Coulomb electrode is $Q_F/2$. Since charges on faces №1 and №2 are opposite, F_{CO} arises. The threshold voltages determine the intensity of the commutation . The Coulomb force F_{CO} can greatly exceed that of F_{CA}. The lifetime of F_{CO} is transient. The disappearance of FCO is determined by the threshold voltages of switch №2. When it switches to ON, the Coulomb electrode is grounded via the R.L.C. circuit which cancels the Coulomb force (Figures 1-6).

Because Coulomb's force F_{CO} is much stronger than the Casimir force F_{CA}, the net force F_{CO} - F_{CA} reverses direction. As the piezoelectric bridge deforms less, fewer mobile electric charges are produced, which in turn lowers the gate voltage V_G . When Switch №2 switches to ON and to the mass , the Coulomb force is neutralized. However, the kinetic energy transferred to both the piezoelectric bridge and the mobile Casimir electrode imparts inertia to the structure, which is gradually dissipated due to the ever-present Casimir force F_{CA}. This allows the deformation of the piezoelectric bridge to continue to decrease and return to its initial position (or even slightly exceed it).

This transient Coulomb force prevents the collapse of the Casimir electrodes and reduces the deformation. The structure returns to initial state or a little above but deforms again under persistent F_{CA} (Figure 2,3).

This process may recur, producing vibrations (see Figures 8-10), where Casimir-induced forces, arising from boundary-condition–dependent vacuum fluctuations, act as an effective interaction within the mechanical dynamics of the system. Casimir-induced forces, arising from boundary-condition–dependent vacuum fluctuations, act as an effective interaction within the mechanical dynamics of the system, without implying any active energy source.

At each cycle, integrated switches №1and №2 redistribute charges on face №1 and №2 of piezoelectric bridge .Initially, the Coulomb electrode is grounded by automatic closure of switch №2 (Figure 2,4).

2. Calculation of the Behavior of the Structure

We calculate the time evolution of the piezoelectric bridge deflection under Casimir force, starting from initial gap z_0 (Figure 2).
Using the angular momentum theorem for this vibrating structure : $\vec{\sigma}^S_{A,x,y,z}$(Structure)= $\bar{\bar{I}}^S_{A,x,y,z}\ \vec{\omega}^S_{A,x,y,z}$ (Eq. 6)

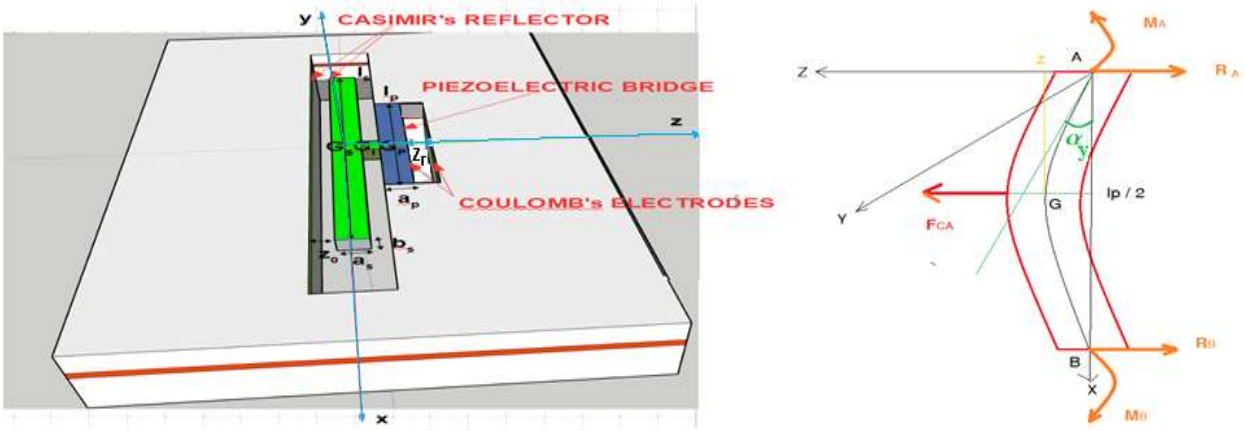

Figure 7: Piezoelectric Bridge Cutting Reactions and Bending Moment, Deflection

$\vec{\omega}^{S}_{Ay} = \begin{pmatrix} 0 \\ \frac{d\alpha_y}{dt} \\ 0 \end{pmatrix}$ with $\frac{d\alpha_y}{dt} \approx \frac{2}{l_p}\frac{dz}{dt}$ since $\sin(\alpha_y) \approx \alpha_y \approx \frac{2z}{l_p}$ for small α_y.(Fig 7)

Let (G_p, x, y, z), (Gi, x, y, z), and ($G_{C,}$ x, y, z) denote the barycenter's of the piezoelectric bridge, connecting finger, and mobile Casimir sole, respectively. $\overrightarrow{AG_{P,x,y,z}} = \frac{1}{2}\begin{pmatrix} l_P \\ b_P \\ a_P \end{pmatrix}$ $\overrightarrow{AG_{I,x,y,z}} = \frac{1}{2}\begin{pmatrix} l_P + l_I \\ b_P + b_I \\ a_P + a_I \end{pmatrix}$ $\overrightarrow{AG_{S,x,y,z}} = \frac{1}{2}\begin{pmatrix} l_P + l_I + l_S \\ b_P + b_I + b_S \\ a_P + a_I + a_S \end{pmatrix}$

The total inertia of the structure becomes , in the reference (A, x, y, z), is : $I^{s}_{A,x,y\,z} = I^{P}_{A,x,\,y,\,z} + I^{I}_{A,\,x,\,y,\,z} + I^{c}_{A,\,x,\,y,\,z}$ With A at the edge of the recessed piezoelectric bridge (figure 7) .

The angular momentum theorem applied to the whole structure gives : $\frac{\overrightarrow{d(\sigma^{S}_{A,x,y,z})}}{dt} = \bar{\bar{I}}^{S}_{A,x,y,z}\,\frac{\overrightarrow{d(\alpha_y)}}{dt} \Rightarrow$

$$\bar{\bar{I}}^{S}_{A,x,y,z}\ \frac{2}{l_P}\begin{pmatrix} 0 \\ \frac{d^2z}{dt^2} \\ 0 \end{pmatrix} = \underset{\Sigma_A}{\rightarrow}\ \overrightarrow{\text{Moments on the structure}} = \underset{M_A}{\rightarrow} + \underset{M_B}{\rightarrow} + \underset{F_{CA}}{\rightarrow} \wedge \begin{pmatrix} l_P/2 \\ 0 \\ 0 \end{pmatrix} \text{ with } \underset{F_{CA}}{\rightarrow} = \begin{pmatrix} 0 \\ 0 \\ F_{CA} \end{pmatrix} \quad \text{(Eq. 7)}$$

The structure rotates around the Ay axis, the moments at point A are $M_{AY} = M_{BY} = -F_{CA}\, lp/8$ [10].

The inertia matrix of the parallelepiped bridge, in the frame of reference (G_p, x, y, z) is (Fig. 7):

$$I^{P}_{GP} = \frac{m_p}{12}\begin{pmatrix} a^2{}_p + b^2{}_p & 0 & 0 \\ 0 & l^2{}_p + b^2{}_p & 0 \\ 0 & 0 & a^2{}_p + l^2{}_p \end{pmatrix} \quad \text{(Eq.8)}$$

Taking Huygens' theorem into account, this inertia matrix becomes (Fig. 7)

$$I^{P}_{A,x,y,z} = m_p\begin{pmatrix} \frac{a^2{}_p + b^2{}_p}{3} & -\frac{l_p b_p}{4} & -\frac{l_p a_p}{4} \\ -\frac{l_p b_p}{4} & \frac{a^2{}_p + l^2{}_p}{3} & -\frac{a_p b_p}{4} \\ -\frac{l_p ba}{4} & -\frac{a_p b_p}{4} & \frac{l^2{}_p + b^2{}_p}{3} \end{pmatrix} \text{(Eq. 9):}$$

With the same reasoning we can calculate the inertia matrix of the parallelepiped finger $I^{I}_{A,x,y,z}$, and the inertia matrix of the reflector $I^{c}_{A,x,y,z}$ in the frame of reference (A, x, y, z),

Any calculation done; we obtain: $I_y^S \frac{2}{l_p}\frac{d^2z}{dt^2} = \frac{l_p}{4} F_{CA} = \frac{l_p}{4} S_s \frac{\pi^2\hbar c}{240z^4}$ with I^S_y the inertia of the structure relatively to the axe Ay.

$$I^S_Y = \rho_P a_P b_P l_P \left(\frac{\left(l_P^2 + a_P^2\right)}{12} + \frac{\left(l_P^2 + a_P^2\right)}{4}\right) + \rho_i a_i b_i l_i \left(\frac{\left(l_i^2 + a_i^2\right)}{12} + \frac{\left(l_P + l_i\right)^2 + \left(a_P + a_i\right)^2}{4}\right) + \rho_s a_s b_s l_s \left(\frac{\left(l_s^2 + a_s^2\right)}{12} + \frac{\left(l_P + l_i + l_s\right)^2 + \left(a_P + a_i + a_S\right)^2}{4}\right) \text{ (Eq. 10).}$$

With ρ_P , ρ_i , ρ_S , respectively the densities of the piezoelectric bridge , the intermediate finger and the mobile electrode of the Casimir reflector .

By equation 7, we obtain the differential equation which makes it possible to calculate the interval between the two electrodes of the Casimir reflector as a function of time during the "descent" from z_0 to z_1 phase when the Coulomb forces are not present . Differential equation for descent phase (so with no Coulomb force) is :

$$\frac{d^2z}{dt^2} = \frac{l_p^2}{8I_{S,y}}\frac{S_S\,\pi^2\hbar c}{240z^4} = \frac{B}{z^4},\ B = \frac{S_s\, l_p^2 \pi^2 \hbar c}{1920\, I_{S,y}} \quad \text{(Eq. 11).}$$

This differential equation n°11 does not have an explicit solution, so we solved it numerically using MATLAB to determine the duration of the “descent” from z_0 to z_1 (fig 8,9,10) . We know that :

1 / as the dispositive move , Casimir force is variable in time, and its equation is (Eq. (1)): $F_{CA} = S_s \frac{\pi^2\hbar c}{240 z_S^4}$

2 / The Coulomb force (Eq 5), variable also over time, acting in opposition to the Casimir force, exist when switch n°1 is ON with : $F_{CO} = \frac{Q_F^2}{4\pi\epsilon_0\epsilon_r}\left(\frac{1}{z_r + z_0 - z_s}\right)^2 = \left[\frac{d_{31} l_p}{a_p} S_s \frac{\pi^2\hbar c}{240}\left(\frac{1}{z_s^4} - \frac{1}{z_0^4}\right)\right]^2 \left(\frac{1}{8\pi\epsilon_0\epsilon_r}\right)\left(\frac{1}{z_r + z_0 - z_s}\right)^2$

The "descent" of the free Casimir electrode must stop when the inter electrode interface z_s reach the position z_1 such that: $\left[\frac{d_{31} l_p}{a_p} S_s \frac{\pi^2\hbar c}{240}\left(\frac{1}{z_s^4} - \frac{1}{z_0^4}\right)\right]^2 \left(\frac{1}{8\pi\epsilon_0\epsilon_r}\right)\left(\frac{1}{z_r + z_0 - z_s}\right)^2 = p\, S_s \frac{\pi^2\hbar c}{240 z_S^4}$ (Eq. (12) See (Fig 18)

This programmable equation n°12 gives the time t_d of the "descent" of the structure submitted to the Casimir force and:

a/ is calculable and will stop when the inter-electrode interface z_s has a value z_1 satisfying equation 12.

b/ depend on the chosen coefficient of proportionality p.

When switch N°1 is ON and switch n°2 is OFF the resultant force applied on the piezoelectric bridge is ; $F_T = F_{CO} - F_{CA} = (1-p)F_{CA} \Longrightarrow (1-p)S_S \frac{\pi^2\hbar c}{240 z_S^4} < 0\ if\ p > 1$ Just at the closing switch n°1 when the Casimir mobile electrode reaches the position z1 (figure 3) , we have $F_{CO} = p\, F_{CA}$ with p , a coefficient of proportionality defined by the threshold voltage of the MOS interrupter №1, which depend on the choosing of the threshold voltage of the TFTMOS of this switch.

We call V_G the TFT MOS grids potential . During $0 < V_{TND} < V_G \leq V_{TNE}$ or $V_{TPE} \leq V_G < V_{TND} < 0$, so when

$$V_{T2} < V_G < V_{T1},\ F_T = F_{CA} - F_{CO} = s_s \frac{\pi^2\hbar c}{240\, z_S^4} - \left[\frac{d_{31} l_p}{a_p} S_s \frac{\pi^2\hbar c}{240}\left(\frac{1}{z_s^4} - \frac{1}{z_0^4}\right)\right]^2 \left(\frac{1}{8\pi\epsilon_0\epsilon_r}\right)\left(\frac{1}{z_r + z_0 - z_s}\right)^2 \quad \text{(Eq. 13).}$$

The piezoelectric bridge subjected to this new force F_T rises towards a position where the Coulomb’s F_{CO} disappears. This occurs at the point z_2 (fig 3), because the switch n° 2 commute and closed to ground via a R.L.C circuit (fig 1,2). When FCO disappears, the whole moving structure (Casimir reflector electrode + finger + piezoelectric bridge) so with an important masse M_t , have acquired a kinetic energy E_C with :

$E_c = \frac{1}{2} M_t V_t^2$ with: $M_t = d_{pm}(a_s b_s l_s + a_i b_i l_i) + 2 d_{om} z_{of}(a_{so} b_{so} + b_{so} l_{so} + a_{so} l_{so}) + d_p(a_p b_p l_p)$

and Vt= speed of the mobile structures , d_{pm} the density of the metal, a_s, b_s, l_s the geometries of the final metal part of the Casimir electrode sole, d_{om} the density of the metal oxide, a_{so}, b_{so}, l_{so} the geometries of the oxidized parts around the 6 faces of the metal blocks, d_p the density of the piezoelectric parallelepiped (see figure 1,2,33):

Let us calculate an approximation of the duration of this "rise" of the mobile electrode Casimir's reflector + finger + piezoelectric bridge , triggered when $F_{CO} = p\, F_{CA}$. This time is calculable because when the Coulomb force F_{CO} stop, then the mobile structure loses its kinetic energy E_c plus its deformation energy submitted at the braking force provided by the Casimir force. In order to simplify the calculus of equation (15) , we approximate this return time by saying that point z_2 (Eq 27) of the loss of the Coulomb force occurs at the initial point z_0 . But , in the same way that we defined point z_1 where Coulomb's force appears, a similar calculation allows us to calculate the point z_2 (Eq 27) where this force disappears . It suffices to calculate the mobile charges $Q_F = Cox\, V_{T2}$ appearing on the TFT MOS gates when the gate voltage V_G reaches the threshold voltage V_{T2} of switch n° 2 , and then we calculate z_2 (see the chapter 4.2.1) with :

$$Q_F = C_{ox} V_{T2} = \frac{d_{31} l_p}{a_p} F_{CA} = \frac{d_{31} l_p}{a_p} s_s \frac{\pi^2 \hbar c}{240\, z_2^4} \qquad \text{(Eq.14)}$$

In these conditions, to know the time taken by the structure to "go back" to its neutral position, we must solve the following differential equation:

$$\frac{d^2 z}{dt^2} = \frac{I_P^2}{8 I_S^Y}\left(F_{CA} - F_{CO}\right) = \frac{I_P^2}{8 I_S^Y}\left\{\left(l_S b_S \frac{\pi^2 \hbar c}{240\, z_S^4}\right) - \frac{1}{2}\left[l_S b_S \frac{\pi^2 \hbar c}{240}\left(\frac{d_{31} l_P}{a_P}\right)\left(\frac{1}{z_s^4} - \frac{1}{z_0^4}\right)\right]^2\right\}\left(\frac{1}{4\pi\varepsilon_0 \varepsilon_r}\right)\left(\frac{1}{z_r + z_0 - z_S}\right)^2 \quad \text{Eq.(15)}$$

This differential equation (15) has no analytical solution and can only be solved numerically. We programmed it on MATLAB. In these MATLAB simulations we considered that the metal of the electrodes and metal block was thermally or by ALD oxidized over a thickness allowing to have an interface between Casimir electrodes of 200 A . This oxidation modifies the mass and the inertia of the vibrating structure (See chapter 5, 6). It turns out that the choice of aluminium as the metal deposited on these electrodes is preferable given:
1 / The ratio between the thickness of the metal oxide obtained and of the metal attacked by a thermal oxidation (see chapter 6).
2 / Its low density increases and optimise the vibration frequency of the structure by minimising the inertia of the Casimir reflector and the parallelepiped block that transfers the Casimir force.

Subjected to the resultant force F_T, the deformation of the bridge decreases and reaches position z_2, where FCO disappears because switch no2 is grounded via the R.L.C. circuit (figure 2). At point z_2 , mobile structure (piezoelectric bridge + Mobile Casimir electrode) acquires kinetic energy $E_C = \frac{1}{2} M_t V_t^2$, with M_t total mass and V_t the speed at point z_2.

We will calculate the final return point z_f (Eq 30) of the piezoelectric bridge + parallelepiped structure of the moving Casimir electrode in Chapter 4, "Energy Balance" .To do this, we will apply the kinetic energy theorem, which rhe cinetiq energy plus the energy acquired by the deformation of the bridge between z_2 and z_f is dissipated by the energy of the Casimir force (F_{CA}).

3. Simulation of Devices with Different Piezoelectric Bridge

We present below the results of the MATLAB simulations carried out by numerically calculating the differential equations (11) and (15). These numerical calculations give the vibration frequency of the structure which vibrates at a frequency lower than its first resonant frequency. This vibration frequency depends on the characteristics of the structure (nature of material, geometric dimensions, coefficient of proportionality $p = F_{CO}/F_{CA}$, etc.
The metal used for the Casimir reflector block is aluminum with a density of 2.7 g/cm³.

3.1. PMN-PT Piezoelectric Materials for the Piezoelectric Bridge

To increase the density of electric charges at the terminals, piezoelectric material PMN-PT can be used. It can be deposited by RF-magnetron sputtering with a composition, for example:
PMN-PT = (1-x) Pb (1/3 Mg - 2/3 Nb) O_3 - x Pb_2TiO_5; with : piezoelectric coefficient $d_{31} = 1450 \times 10^{-12}$C / (kg m s^{-2}) and a Young's modulus $E_p = 150 \times 109$kg m^{-1} s^{-2}. With MATLAB simulation, and for an interval between Casimir electrode $z_0 = 200$Angstroms, we obtain the evolution over time of the Casimir and Coulomb forces as well as the F_{CO}/F_{CA} ratio of figures 8 to 17 below. For a ratio p

= F_{CO} /F_{CA} of 1000, the maximum current I delivered by the vibrating structure, the threshold voltage of the MOSE and the vibration period of the structure are respectively: I = 1.2 × 10^{-4}A, V_t = 3.2V and a period of vibration of 3.012 10-6 so a frequency of 332005 Hertz (figure 9)

3.1.1 Evolution of the Casimir Interface as a Function of Time During Two Periods: PMN-PT

The F_{CO} /F_{CA} ratio = 10000 induces a period of 3.85 × 10^{-6}s and a rise time of 21.3 × 10^{-9}s with a deflection of the bridge of 105 Å. The structure vibrates at 259 kHz. Due to inertia, at the rise sequence, the structure exceeds the initial 200 Å by 20 Å (Fig 8 ,15, 20).

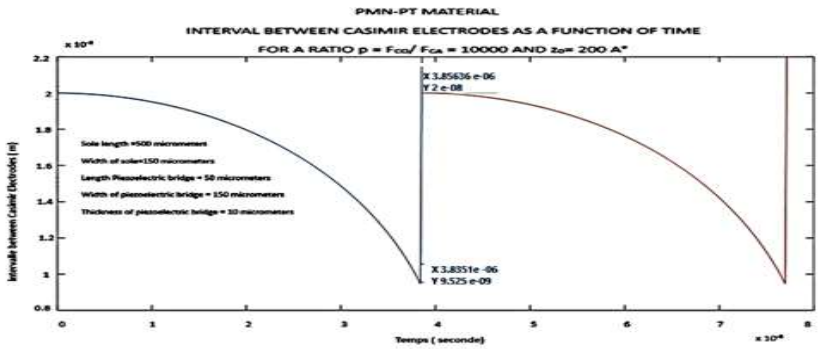

Figure 8: Plot of the Evolution of the Casimir Inter-electrode Interval as a Function of Time Over Two Periods and an FCO/FCARatio = 10000: Casimir Inter-Electrode Interface = 200 Å

A ratio F_{CO} /F_{CA} = 1000 induces a period of 3.012 × 10^{-6}s and a rise time of 44.5 × 10^{-9}s with a deflection of the bridge of 50 Å. The structure vibrates at 320 kHz: (fig 9). For this ratio of 1000 we notice a vibration amplitude of 50Å, a period of 2.96 × 10^{-6}s, with the faster rise of the mobile electrode producing a slight rebound of 5Å, because of the inertia of the structure.

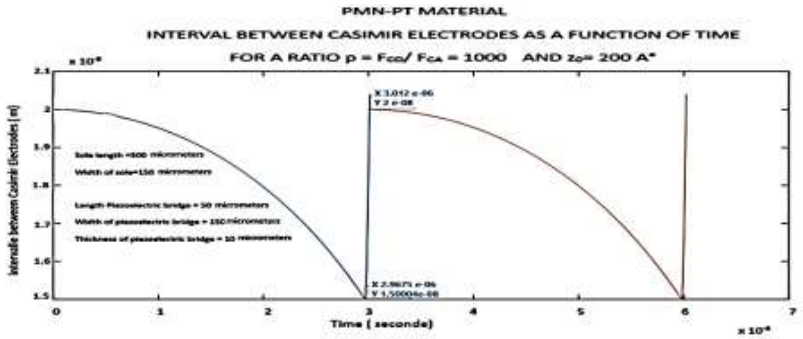

Figure 9: Plot of the Evolution of the Casimir Inter-electrode Interval as a Function of Time Over Two Periods and FCO/FCARatio = 1000: Casimir Inter-Electrode Interface = 200 Å.

For the ratio FC_0 / F_{CA} = 2(figure 10) a vibration amplitude of just 0.27 Å and a period of 1.93 × 10^{-7} s is obtained, so a frequency of about 5.2 Mhz . This low deformation of the PMN-PT piezoelectric bridge is mainly due to the extremely high piezoelectric coefficient d_{31} of 1450 (pC/N) of PMN-PT compared to 120 (pC/N) for PZT.
We observe the weak overshoot of the initial interface.

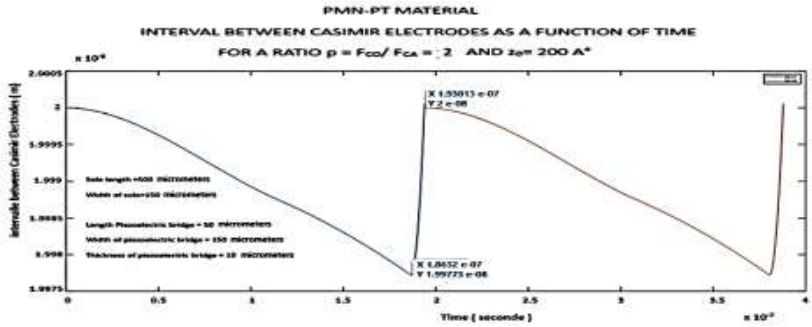

Figure 10: Plot of the Evolution of the Casimir Inter-electrode Interval as a Function of Time Over Two Periods and a Ratio FCO/ FCA=2. Casimir Inter-electrode Interface = 200 Å

3.1.2 Evolution of the Forces of Casimir and Coulomb: PMN-PT

We obtain: 1/ The evolution of the Casimir and Coulomb forces as a function
a / of the inter-electrode interface (figure 11) and
b/ over time (figure 12)
2/ The F_{CO} / F_{CA} ratio as a function of time for an entire period (figures 13).

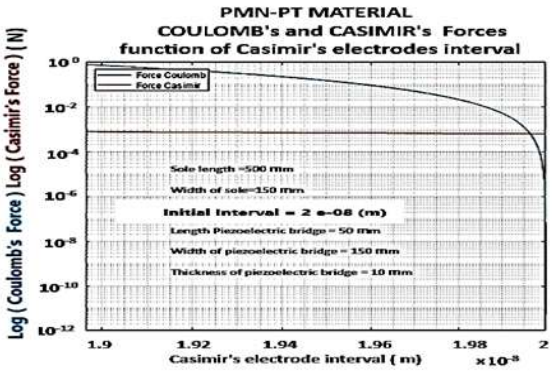

Figure 11: Materials = PMN-PT: Coulomb and Casimir Force as a Function of the Inter-electrode Interface. Start Interface = 200A °

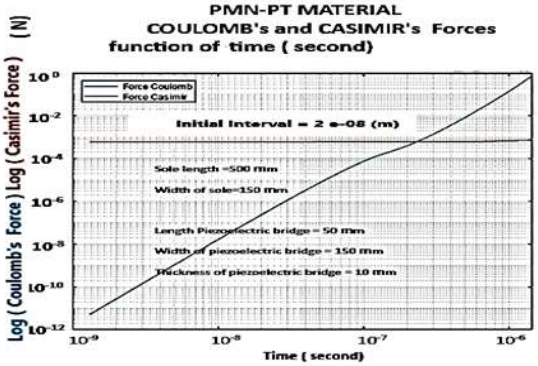

Figure 12: Materials = PMN-PT: Coulomb and Casimir Force as a Function of Time. Start Interface = 200A °

It is observed (Figure 13) that the Coulomb return force is less important for an initial inter-electrode gap z_r = 400Å than for z_r = 200Å

Figure 13: Materials = PMN-PT: Coulomb Force for z_r = 200Å (Blue) and z_r = 400Å (Red) and Casimir Force (Yellow, z_0 = 200Å) as a Function of the Inter-electrode Interface Starting Interface = 200 Å.

We observe the gradual evolution towards the chosen ratio p = F_{CO} / F_{CA} of 450 and then the sudden drop in this ratio as the electrodes regain their initial position (Fig. 14). The break circuits n°1 triggered at time t = 2.44 10^{-6} s suddenly induce a rise of the mobile electrode the deformation of the piezoelectric bridge sharply decreases, therefore a sudden decrease in electric charges and grids voltages

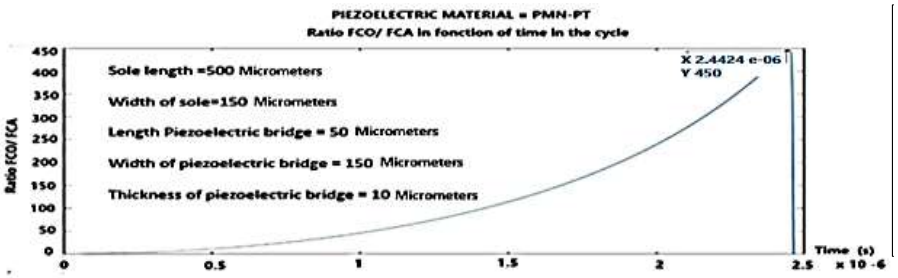

Figure 14: Materials = PMN-PT: Ratio p = F_{CO} / F_{CA} as a Function of Time, During a Period of Vibration. Start Interface = 200A °, Maximum Ratio Chosen = 450

3.1.3 Threshold Voltage According to the Desired Ratio Fco / Fca: PMN-PT

It can be seen (Fig. 15) that we increase the threshold voltage of the TFT MOS of switch n°1 up to 3.5V if we desire to obtain a ratio F_{CO} / F_{CA} of 1000.

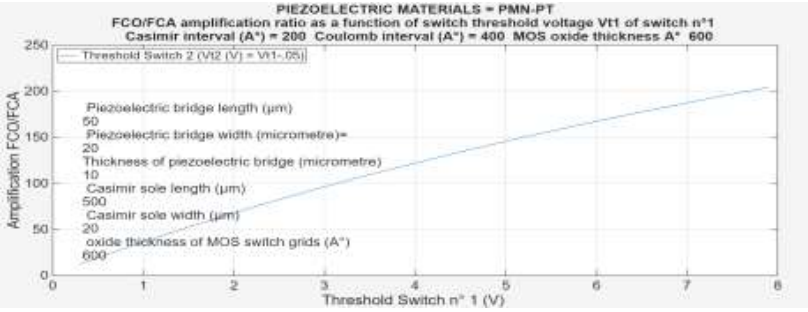

Figure 15: Materials = PMN-PT: Threshold Voltage of Enriched MOS Transistors Voltage (V) in Function of Ratio Fco / Fca, Start Interface = 200A

3.1.4 Vibration Frequency as a Function of the Fco / Fca Ratio and Peak Current as a Function of the Initial Casimir Interval Chosen: PMN-PT.

Note that for an initial interface z_0 = 200 Å and for a ratio Fco / Fca = 2, the maximum vibration frequency of the structure is 5.10 MHz. It falls to 750 kHz for a ratio of 1000. These frequencies are still lower than the first resonance of the structure, which is of the order of 7.94 Megahertz. This vibration frequency of the Casimir structure approaches that of the first resonance for weaker interfaces below 200 Å.

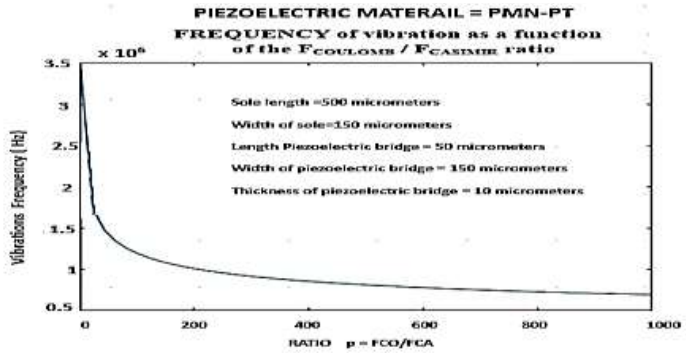

Figure 16: Materials = PMN-PT: Vibration Frequency as a Function of the Fco / Fca Ratio, Start Interface = 200A

The (Figure 17)shows the evolution of the peak current obtained for a ratio Fco / Fca = 500. The maximum current delivered by the structure falls as a function of an increase in the initial Casimir interval.

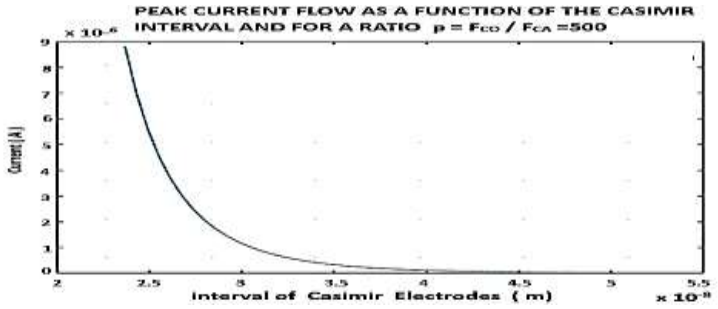

Figure 17: Materials = PMN-PT: Current Peak Across the 2 . 10-4 H Inductance as a Function of the Starting Interval Between Casimir Electrodes. Start Interface = 200A° Ratio F_{CO} / F_{CA}= 500

It seems that the piezoelectric material PMN-PT coupled with a conductor like aluminum is an interesting couple for our vacuum energy interaction structure.

4. Mems Energy Balance

In this part, we will try to make a detailed and exhaustive assessment of the behavior of the MEMS during one vibration. Initially, our attention will be directed towards the initial portion of this vibration, referred to as the "go" phase (from z0 to z1). Secondly, we will focus on the second half of the vibration, which is to say the "return" phase(Figure 3) . Recall that we assume the piezoelectric bridge is perfectly elastic, meaning any energy used to deform it from position 0 to 1 is fully recovered when returning from 1 to 0. The conditions of use of the piezoelectric bridge (vibrations amplitude) are in the purely elastic domain, and we never enter in the domain of plasticity.

In the following we propose to put into equation the energy balance of «go» then in "return" steps , with p the chosen amplification $p = F_{CO} / F_{CA}$.

We have : $\mathbf{0 < V_{TPD} < V_{TNE}}$, **and** $\mathbf{V_{TPE} < V_{TND} < 0}$ **and** $\mathbf{F_{CO} / F_{CA} < p}$. We define VT1 as the absolute value of either VT_{NE} or VT_{PE}, and V_{T2} as the absolute value of either VT_{ND} or VT_{PD} ,(Fig 4) . V_G refers to the voltage that arises from the mobile charges on the second surface of the piezoelectric bridge and appears at the gate of all TFT MOS transistors. [11] fig 1,2 . Recall that the threshold voltage V_{T2} of switch №2 is a little less than the threshold voltage V_{T1} of switch №1, and that V_{T2} equals V_{T1} minus a few tens of millivolts. (Figure 4)

4.1. MEMS Energy Balance During the Phase "go" From z0 to z1

a/ $\mathbf{0 < V_G < abs(V_{T2}) < abs(V_{T1})}$ **and** $\mathbf{F_{CO} / F_{CA} < p}$**: switch n°1 OFF, Switch n°2 ON. (Fig 1,2, 4)**

At the start, in the beginning conditions of the "go" phase, we have very small deformations applied to the piezoelectric bridge. Consequently, very small electrical charges are present on it, so the electrical voltages V_G on the grid of the enriched and parallel TFT MOS N and P of switch N°1 is lower than their threshold voltage V_{T1}. This switch n°1 is open and in the OFF position. On the other hand, as $V_G < V_{T2}$, switch N°2 consisting of two TFT MOS N and P in series, operating in depletion mode is closed and in the ON position to ground.

In these conditions the so-called Coulomb electrode is to the ground, thus eliminating the Coulomb force F_{CO}.

b/ $\mathbf{0 < abs(VT_2) < VG < abs(V_{T1})}$**. and** $\mathbf{F_{CO} / F_{CA} < p}$**: switch n°1 OFF, Switch n°2 OFF. (Fig 1,2, 4)**

No moving electric charge appears on the return side of the Coulomb electrode which is isolated of ground by switch №2 which is OFF, and isolated from the piezoelectric bridge by switch №1, which is also OFF.

As the Casimir force increases, it causes greater deformation of the piezoelectric bridge. Consequently, the electric field created by the difference in its barycenter of ionic charges causes inverse mobile charges to accumulate on faces 1 and 2 of the piezoelectric bridge. This accumulation increases the gate voltage (V_G) for the transistors in switches 1 and 2. This voltage V_G still lower than the threshold voltage V_{T1}, exceeds now V_{T2} of switch №2 which opens and switches OFF.

The structure being assumed to be perfectly elastic and the amplitudes of the vibrations being extremely low, we will see that the mechanical energy losses by an increase of temperature in the device are negligible.

1/ Note also that the mobile parallelepiped metal electrodes of the Casimir electrodes remain parallel to each other and that the mobile metal Casimir electrode does not deform therefore does not heat up. It simply transmits its movement by the finger to the piezoelectric bridge which deforms (Figure 1,2)
2/ The expulsion of entropy ΔS from the vibrating structure of Casimir is transmitted to the piezoelectric bridge. It causes an extremely slight increase ΔT in its temperature and expels this heat to the outside.

Let us calculate an order of this magnitude ΔT. We note ΔQ_{vib} the heat transmitted by the vibrations of the piezoelectric bridge. In first approximation, we can use the well-known formula $\Delta Q_{vib} = \Delta S \cdot \Delta T$, with: ΔS = entropy variation ($J \cdot K^{-1}$) and ΔT = temperature variation (°K)

However, we know that: $\mathbf{\Delta Q_{vib1}} = (M_{Bridge} [2\pi f_{vib1}]^2 / 2) (z_0\text{-}z_1)^2$. Eq. (16) [10]
With: f_{vib} = Vibration frequencies of the piezoelectric bridge for an amplitude of $z_0\text{-}z_1$, M_{Bridge} = mass of the piezoelectric bridge, which is the only one to deform because the Casimir electrodes are simply in translations. We note z_1 the maximum deflection of the bridge (Fig 3). This heat expended at the level of the piezoelectric bridge causes its temperature to increase.

As a first approximation we can say: $\Delta Q_{vib} = M_{Bridge} \cdot C_{piezo} \Delta T$.
With: C_{piezo} = Specific heat capacity of the piezoelectric bridge ($J\ Kg^{-1} \cdot K^{-1}$), ΔT = Temperature variation (°K).

Consequently $\Delta T_1 = (2 [\pi f_{vib1}]^2 / C_{piezo}) (z_0\text{-}z_1)^2$ = Temperature variation of the bridge. Eq. (17)

For example, for a PMN-PT piezoelectric film: $C_{piezo} = C_{PMN\text{-}PT} = 310$ ($J\ Kg^{-1} \cdot K^{-1}$), $f_{vib} \approx 106$ Hz, $z_0\text{-}z_1 \approx 100 \times 10^{-10}$ m. We therefore obtain: $\Delta T_1 \approx 10^{-3}$ K.

In conclusion, the expulsion of entropy from the vibrating Casimir electrode is negligible. We note that simply half of this expended heat occurs in the “go”, the second part occurs in the “return” phases of the vibration.

Throughout the cycle from z_0 to z_1, the deformation of the elastic piezoelectric bridge during the "go" phase of vibration utilizes the energy provided by the Casimir-induced mechanical deformation. It is critical to note that the system does not extract energy from the quantum vacuum itself. Instead, the Casimir force acts as a conservative mechanical driver, while the usable energy results from the conversion of mechanical deformation into electrical energy via the piezoelectric effect and synchronized charge commutation. This energy is applied across four distinct forms.

1/ The mechanical energy for the deformation of the simple elastic bridge: $\mathbf{W_{DEFCA}}$
2/ The energy to create the fixed QF charges in this piezoelectric structure : $\mathbf{W_{BRIDGE}}$
3/ The energy for the simple displacement of the point of application of the Casimir force in the middle of the bridge : $\mathbf{W_{CASIMIR}}$
4/ The expulsion of entropy ΔS/2 energy, expended in heat due to the friction of the atoms in the half of the vibration of the bridge heat : $\mathbf{\Delta_{Qvib}\ /2}$

We obtain the relation $\mathbf{E_{CASIMIR} = W_{DEFCA} + W_{BRIDGE} + W_{CASIMIR} + \Delta Q_{vib}\ /2}$

We can write that to deform the piezoelectric bridge from the start position z0 to the position z1 :

$\mathbf{E_{CASIMIR1} = W_{DEFCA1} + W_{BRIDGE1} + W_{CASIMIR1} + \Delta Q_{vib1}\ /2,}$ (Eq 18).

The quantum vacuum energy, labeled $E_{CASIMIR1}$, is larger than the basic translation energy, $W_{CASIMIR1}$, related to the Casimir force F_{CA}. The energies W_{DEFCA1} and $W_{BRIDGE1}$ are stored as potential energy in the piezoelectric bridge that has been deformed to position from z_0 to z_1.

This distinction is significant because it suggests that, in theory, the system enables a redistribution of energy between mechanical and electrostatic degrees of freedom, without implying any net extraction of energy from the vacuum. Even though the Casimir force is conservative - which means the energy required for displacement is the same both ways, between points 0 and 1- the scenario described here is different: the vacuum energy causes deformation of a fixed piezoelectric bridge and exceeds the energy involved in simply moving the point of application of the Casimir force. The bridge then returns to its original state due to a self-induced, opposite, temporary Coulomb force of greater intensity. Ultimately, only part of the deformation energy stored in the piezoelectric bridge is recovered, appearing as a peak in electrical power output.

1/ The translation energy of the Casimir force is:

$$\mathbf{W_{CASIMIR1}} = \int_{Z_0}^{z_1} F_{CA}\, dz = \int_{Z_0}^{z_1} S\ \frac{\pi^2\ \hbar\ c}{240\ z_s^4} dz_S = S\left(\frac{\pi^2\ \hbar\ c}{720}\right)\left[\frac{1}{z_1^3} - \frac{1}{z_0^3}\right].\ \text{(Eq 18)}$$

The WCASIMIR1 energy represents the translation of the Casimir force F_{CA} from z_0 to z_1 but without considering that this force also deforms an elastic and piezoelectric structure from z_0 to z^1.

Now, let's calculate the deformation energy W_{DEFCA} of the piezoelectric bridge fixed at both ends.

We know that the deformation energy of an elastic system is the energy that accumulates in the solid body during its elastic deformation. Yet all Material Resistance books say that the deformation energy W_d of an recessed elastic bridge and for a constant force F is : Wd = 1/2 z_e F, with $z_e = z_0$ - zs, the deflection (arrow) acquired by the elastic bridge subjected to the constant force F.

In the case of our piezoelectric bridge the force F being the Casimir force, varies in 1/z^4, with the distance z.

So, for a differential deflection dz of the bridge under the force F(z) we can write

$$d(W_d) = 1/2\ F(z)\ dz \implies W_d = W_{DFCA}(z_1) = \frac{1}{2} S\ \frac{\pi^2\ \hbar\ c}{240} \int_{z_0}^{z_1} \frac{1}{z^4}\ dz\ = S\ \frac{\pi^2\ \hbar\ c}{1440}\left[\frac{1}{z_1^3} - \frac{1}{z_0^3}\right] \text{(Eq 19)}$$

The strain energy $W_d = W^{DEFCA}$ is stored in the elastic bridge as potential energy and is used to straighten the piezoelectric bridge, together with the energy of a Coulomb force originating from $W_{BRIDGE1}$, thereby providing kinetic energy to the entire structure.

The position of the mobile Casimir electrode reaches the limit z_1 when the grid voltage V_G on switch n°1 reaches its threshold voltage V_{T1} . This reached position z_1 is unstable because the Casimir force increases with its position. As a result, the mobile Casimir electrode can collapse. But, when the Casimir electrode is in position z_1 , the switch n°1 switches to ON . The charges present on the metallic face n°1 of the piezoelectric bridge must homogenize with the metallic Coulomb electrode (there is no electric field in a perfect conductor) , which was previously grounded by the closing of switch n°2 . Note that, when switch n°1 switches, switch n°2 is still OFF because the TFT MOS of switch n°2 are in depletion and $V_G > V_{T2}$ (Fig 1,2,3,4).

The energy stored in the bridge through its deformation is in z_1 : $\boldsymbol{W_{DFCA1}} = \frac{1}{2}\, S\, \frac{\pi^2\, \hbar\, c}{720} \left[\frac{1}{z_1^3} - \frac{1}{z_0^3}\right]$ Eq. 20,

At position z_2 of annulation of the Coulomb's force the memorized elastic energy is :

$\boldsymbol{W_{DFCA2}} = \frac{1}{2}\, S\, \frac{\pi^2\, \hbar\, c}{720} \left[\frac{1}{z_2^3} - \frac{1}{z_0^3}\right]$ Eq.21 . We notice that $W_{DEFCA} > 0$ and that the numerical value of W_{DEFCA1} is a little smaller than the expression calculated when FCA(z1) was constant : Wd= ½ z1 *$F_{CA}(z_1)$ = $\boldsymbol{W_d} = \frac{1}{2} S\, \frac{\pi^2\, \hbar\, c}{240} \left[\frac{1}{z_1^3} - \frac{1}{z_0^3}\right]$ which is consistent .

2/ During the displacement "go" the energy ECASIMIR is also used to generate a potential energy WBRIDGE accumulated in the capacity of the piezoelectric bridge which follows the equation:

$d(W_{BRIDGE}) = QF\ d(V_{PIEZO})$ with V_{PIEZO} = Voltage between the two metallic faces of the piezoelectric bridge, and $Q_F = C_{PIEZO}\ V_{PIEZO} \Rightarrow$ $W_{BRIDGE1}$ = potential energy at the position z_1 which added to W_{DFCA1} and create the coulomb's force.

$$\boldsymbol{W_{BRIDGE1}} = \int_0^{Q_1} Q_F\, d(V_{PIEZO}) = \int_0^{Q_1} \frac{Q_F}{C_{PIEZO}}\, d(Q_F) = \left[\frac{Q_F^2}{2\, C_{PIEZO}}\right]_0^{Q_1} = \frac{a_P}{2\ l_P b_P \epsilon_0\, \varepsilon_{PIEZO}} \left(\frac{d_{31}\, l_p}{2\, a_P}\right)^2 F_{CA}^2 = \left(\frac{a_P}{2\ l_P b_P \epsilon_0\, \varepsilon_{PIEZO}}\right) \left(\frac{d_{31}\, l_p\, l_s b_s\, \pi^2 c\, \hbar}{480\, a_P}\right)^2 \left[\frac{1}{z_1^4} - \frac{1}{z_0^4}\right]^2$$ Eq. (22)

We notice that $W_{BRIDGE1} > 0$, similarly when the structure reaches position z_2 , the same memorized elastic energy occurs. To get $W_{BRIDGE2}$ for position z_2 of the bridge, we simply swap z_1 for z_2.

$$\boldsymbol{W_{BRIDGE2}} = \left(\frac{a_P}{2\ l_P b_P \epsilon_0\, \varepsilon_{PIEZO}}\right) \left(\frac{d_{31}\, l_p\, l_s b_s\, \pi^2 c\, \hbar}{480\, a_P}\right)^2 \left[\frac{1}{z_2^4} - \frac{1}{z_0^4}\right]^2$$

In these equations, we use $d(Q_F) = C_{PIEZO}\ d(V_{PIEZO})$, with C_{PIEZO} = electrical capacity of the piezoelectric bridge, $C_{PIEZO}\ \frac{\epsilon_0\, \varepsilon_{PIEZO}}{a_P} b_P l_P$ Eq.23 and ε_{PIEZO} the relative permittivity of the piezoelectric bridge (Fig 1,2).

We know (Eq 2) that the creating fixed charges on this piezoelectric structure is $Q_F = \frac{d_{31} l_P}{a_P} F_{CA}$

We have $Q_e = - Q_F$ = the accumulated mobile charges, coming from the mass, on the surface of the metallic film.
This part W_{BRIDGE} of energy must provide from the energy of vacuum $E_{CASIMIR}$ and is stored in the piezoelectric bridge as potential energy. It contributes to the usable energy $W_{ELECTRIC}$ appearing during a cycle of vibration of the bridge. So, during the phase "go" from z_0 to z_1 the total Energy associated with Casimir-induced interaction during the cycle = $E_{CASIMIR}$ is used:
1/to deform the piezoelectric bridge with the energy WDEFCA1, 2/ to produce the electrical charges as potential energyWBRIDGE1,
3/Translate the point of application of the Casimir Force WCASIMIR1,
4/ produce a heat of the structure by the entropic transfer ΔQ_{vib} /2 .

So, we have: Energy associated with Casimir-induced mechanical deformation during the 'go' phase can be written: $\mathbf{E_{VACUUM1} = W_{DFCA1} + W_{BRIDGE1} + W_{CASIMIR1} + Q_{vib1}/2}$ (Eq 24)

W_{DEFCA1} and $W_{BRIDGE1}$ are potential energies that will be used when the elastic bridge returns to its equilibrium position, that is to say without deformation. As the Casimir force is conservative, the energy $W_{CASIMIR1}$ is conserved and is not used from the return phase .

4. 2. MEMS Energy Balance During the "Return" Phase from z_0 to z_1" , Switch n°1 ON, Switch n°2 OFF: 0 < abs (V_{T2}) < V_G > =abs (V_{T1}). and Ratio F_{CO} / F_{CA}> = p: (Figure 1)

Figure 15 on page 10 above presents the F_{CO} / F_{CA} ratio, which results from selecting the threshold voltage V_{T1} of switch n°1 during the technological implementation of the MEMS. Now , the voltage on the grids of switch n°1 exceed its threshold voltage and switch n°1 commute ON. The switch n°2 is till OFF, so the Coulomb's electrode is opened .

The free charges Q_{m1}, stored on the metal electrodes of face 1 (Figure 1,4,5), are obliged to go through one of the MOSE transistors N or P , and are uniformly distributed on the Coulomb metal electrode of the surface S_{C1} for example.

If S_{C1} = S_{P1}= lp*bp , this metallic Coulomb's electrode therefore has approximately a mobile charge Q_{mn} S_{C1} / S_{P1} = Q_{mn}/2. This homogenization of electrical charges is obligatory because there is no electric field in a perfect metallic conductor. The free charges Q_{m2}, stored on face 2 of the bridge and on all the isolated grids TFT MOS don't move. So, grids electrode and return Coulomb's electrode have opposite free charge. (Figure 1,4,5).

A Coulomb force F_{CO} then appears between these two electrodes during the very short time when switch no. 2 is still open, isolating the Coulomb electrode from the ground.

A resultant force F_R = F_{CO} - F_{CA} is then applied to the piezoelectric bridge. Depending on the value of the threshold voltage $V_{T1,}$ this force F_R is opposed to the force F_{CA} or to the zero limit. When the force F_R is applied, both the bridge's deformation and its electrical charges are reduced , resulting in a necessary reduction of grid voltages. Since the threshold voltage V_{T2} of switch n°2 is lower but very close to V_{T1} (we choice V_{T1} – V_{T2} = 50 mV on the simulation), the time duration during which this Coulomb exerted force is very small (a few nanoseconds). Very quickly, the switch n°2 commutes another time from OFF to ON, grounding the Coulomb electrode via an R.L.C. circuit, (Fig 21). The Coulomb force vanishes quickly after its appearance at position z_2. The values of V_{T2} and V_{T1} impose that z_2 is very close to z_1. So , the energy $W_{COULOMB} = \int_{z_1}^{z_2} F_{CO} dz$ expended by the Coulomb force remains low, even if this force is several times that of Casimir in intensity.

The time of existence of FCO is of the order of a few tens of nanoseconds (fig 1,5). The position z1 of appearance of this force FCO is such that FCO = p FCA and is numerically calculated by MATLAB(fig. 18) by solving numerically the equation $F_{CO}=pF_{CA} \Rightarrow \frac{Q_F\ Q_F}{8\,\pi\,\varepsilon_0\,\varepsilon_r}\left(\frac{1}{z_r+z_0-z_S}\right)^2 = \left[\frac{d_{31}\,lp}{ap} S_S \frac{\pi^2\,c\,\hbar}{240}\left(\frac{1}{z_S^4}-\frac{1}{z_0^4}\right)\right]^2 \left(\frac{1}{8\,\pi\,\varepsilon_0\,\varepsilon_r}\right)\left(\frac{1}{z_r+z_0-z_S}\right)^2 = p\,S\,\frac{\pi^2\,c\,\hbar}{240\,z_S^4}$ (Eq 25).

We note that the mobile electrical charge are:

1/ Q_F on the face 2 of the piezoelectric bridge and only Q_F/2 on the Coulombs' electrode and

2/ The position z1 depends on the values of the interface zo of the Casimir electrodes and the Coulomb electrodes zr and can be easily calculated in MATLAB for example, see figure 18 below

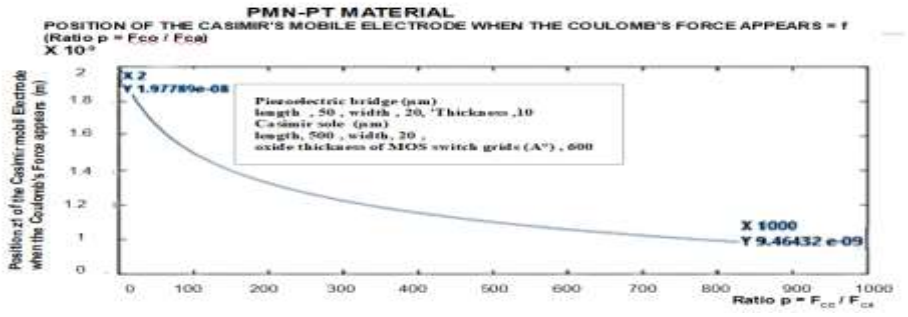

Figure 18: Position of the mobile Casimir electrode z1 where the Coulomb force occurs : z_r = z_0 =200A°, ls = 500 µm, bs = 20 µm, lp = 50 µm, bp =20µm, ap = 10µm

The F_R= F_{CO} - F^{CA} force is now applied to the mobile structure. This resulting force is at least zero or has a greater intensity than the Casimir force F_{CA}. It helps to strengthen the structure and imparts kinetic energy to the mobile structure, by utilizing the energy stored in the elastic bridge . This FCO force exists as long as switch n°2 has not switched to ground, canceling its existence by the dispersion of

charges on the Coulomb electrode. We describe below the energy dispensed in the cycle of the piezoelectric bridge positions. We hope show that a usable energy WELECTRIC is possible to use and not due to any electrical energy applied but only by the dissipation of the mobile electric charges to the mass throw the switch n°2 and an R.L.C. circuit.(Fig 21)

The following section provides a detailed account of the energy distribution throughout the return cycle of piezoelectric bridge positions from z_1 to z_f with z^f the final position of the bridge .

There are two phases for this return to from z_1 to z_f (returning phase):
1/ from z_1 to z_2 where the Coulomb force F_{CO} exists and contributes to straightening the elastic structure and giving kinetic energy to the moving structures,
2/ from z_2 to z_f where this acquired kinetic energy, and the remaining energy $\mathbf{W_{DEFCA2}}$ still stored in the structure which will be dissipated by the energy spent by the Casimir force.

4.2.1 Calculation of Energies Between z_1 and z_2

As soon as switch n°1 has switched to homogenize the electric charges between face 1 of the bridge and the Coulomb electrode, the resulting force F_{CO} - F_{CA} straightens this bridge, and the electric charges drop on the grid of the TFT MOS . The electric voltage on the grids falls very quickly below the threshold voltage of this switch n°1 which commute again very quickly from ON to OFF.

As the threshold voltage of the switch n°2 V_{T2} is lower than the threshold voltage of the switch n°1, V_{T1}, the switch n°2 is still OFF and the Coulomb electrode is isolated . Therefore, two things occur :

1/ Moving charges flow from the ground to face n°1 to balance those on face n°2. These charges originating from ground and passing through a solenoid generate a voltage peak, such as a positive one. This peak voltage feeds the input of the circuit designed to convert these transient power peaks into a stable positive DC voltage relative to ground (fig 1,2) .

2/ The Coulomb force F_{CO}, opposite to F_{CA}, is therefore present between the completely isolated Coulomb electrode and the electrode on face n°2 of the piezoelectric bridge. The resulting force F_{CA}-F_{CO} rectifies the bridge, so its electrical charges decrease, and therefore the gate voltage of the transistors decreases. This causes the depleted transistors of switch n°2 to switch ON. Consequently, the Coulomb electrode is connected to ground through an RLC circuit. As these charges flow towards ground throw an RMC circuit , they generate a voltage peak inverse to the previous one at the terminals of the solenoid, resulting in a negative voltage peak, for example.

The circuit for autonomously converting voltage peaks into DC voltage is thus powered by positive and negative voltage peaks. The energy $W_{COULOMB}$ is write Eq26:

$$\mathbf{W_{COULOMB}} = \int_{z_2}^{z_1} F_{C0}\, dz = \left\{ S_S \cdot \frac{\pi^2 \, \hbar \, c}{240} \cdot \frac{d_{31}\, l_p}{a_p} \right\}^2 \left(\frac{1}{8\,\pi\epsilon_0\,\epsilon_r} \right) \cdot \int_{z_2}^{z_1} \left[\left(\frac{1}{z_s{}^4} - \frac{1}{z_0{}^4} \right) \left(\frac{1}{z_r + z_0 - z_s} \right) \right]^2 dz_s \quad \text{Eq.26}$$

This energy only exists between the very close positions z1 and z2 of the piezoelectric bridge. A literal formulation of WCOULOMB energy is possible but its expression is not convenient because it is too complex. We prefer to calculate by MATLAB its numerical value between the value z_1 and z_2. The position z_2 of commutation of switch n°2 is deduced from the chosen threshold value V_{T2} of switch n°2. We note that we can minimize the value of the energy spent by WCOULOMB, by choosing a value of the threshold voltage V_{T2} close but slightly lower than V_{T1} of switch n°1. For example, $V_{T2} = V_{T1}$- 0.05 (V). We use MATLAB to find position z_2 of commutation of circuit 2 to cancel the Coulomb's Force F_{CO}, see (Eq 22) and figure 18. At position z_2 of the bridge, the electric charge in the TFT MOS is

$$Q_2 = \frac{d_{31}\, l_p}{a_p}\, S_S\, \frac{\pi^2\, c\, \hbar}{240} \left(\frac{1}{z_2^4} - \frac{1}{z_0^4} \right) \text{ with } Q_2 = Cox\, V_{T2} \text{ . We deduce } , z_2 = \frac{1}{\sqrt[4]{\left[\frac{240\, a_p\, C_{ox}}{d_{31}\, l_p\, \pi^2\, c\, \hbar\, S_S} V_{T2} + \frac{1}{z_0^4} \right]}} \quad \text{(Eq .27).}$$

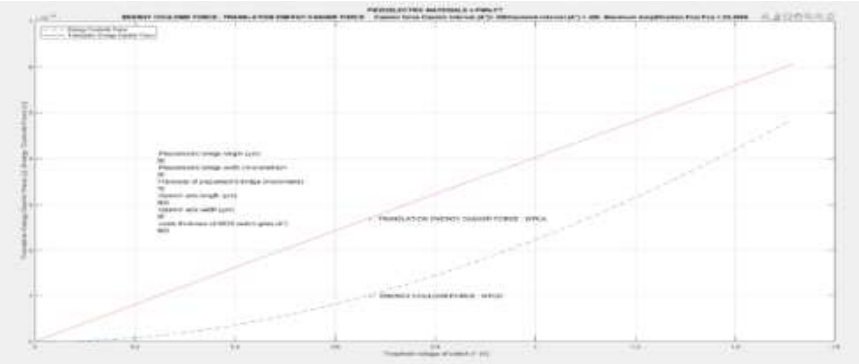

Figure 19: Energy of translation of Casimir Force and energy of Coulombs 'Force between its apparition in the position z_1 and its disappearance in position z_2

We present in figure 19 the curve representing the translation energy $W_{CASIMIR1}$ of the Casimir force, as well as the Coulombs energy $W_{COULOMB}$ during the time when the structure is between the positions z_1 and z_2, which represents a few nanoseconds.

We can calculate the energy spent in the first part of return of the structure (from z_1 to z_2), by simply calculating the kinetic energy W_{CIN} acquired by the structure when it reaches the position z_2 upon its return and by applying the kinetic energy theorem. We know that the variation of the kinetic energy W_{CIN} is equal to the sum of all the energies (internal and external) supplied or spent on the moving structure. Thus, as we know, the numerical value of all these participants, we can calculate that the kinetic energy W_{CIN}, acquired at the position z_2 is the variation of all the energies between the positions z_1 and z_2 .

So, we can write equation Eq.28 which allows us to calculate W_{CIN} because all the terms of this equation are known.

$$\mathbf{W_{CIN1} = [(W_{DFCA1} + W_{BRIDGE1}) - (W_{DFCA2} + W_{BRIDGE2})] + W_{COULOMB} - (W_{CASIMIR1} - W_{CASIMIR2})} \quad \text{(Eq. 28) and fig 20.}$$

With all the terms of the above equation known, we now know the kinetic energy acquired by the entire moving system at z_2 since we know when the Coulomb force disappears at z_2. All calculations done, we obtain :

$$W_{CIN1} = S\,\frac{\pi^2\ \hbar\ c}{240}\,\frac{1}{6}\left(\frac{1}{z_1^3} - \frac{1}{z_2^3}\right) + \left(\frac{a_P}{2\ l_p b_P \epsilon_0\ \varepsilon_{PIEZO}}\right)\left(\frac{d_{31}\ l_p\ l_s b_s\ \pi^2 c\ \hbar}{480\ a_P}\right)^2\left[\frac{1}{z_1^4} - \frac{1}{z_2^4}\right]^2 + W_{COULOMB} \quad \text{(Eq.29)}$$

We know now the kinetic energy W_{CIN1} acquired in point z_2 and the position where the Coulomb z_2 force disappears.

The structure must now dissipate the energy that gives its inertia common to all moving structures. The braking energy provided solely by the Casimir force must cancel this kinetic inertia, augmented by the inertia stored in elastic energy W_{DFCA2}. Let us calculate the final ascent position z_f of the mobile structure.

We have the inertia provided by the kinetic energy W_{CIN1}, a stored elastic energy W_{DFCA2} , a stored electric energy $W_{BRIDGE2}$ and the mobile structure is slowed down by the energy provided by the Casimir force. We can simply write the kinetic theorem of energy between the position z_2 with the kinetics' energy W_{CIN1} , and z_f where this energy disappears. Of course, we must consider that the moving system lost the electrical energy provided in the RLC circuit through the evacuation to ground of the mobile charges from the Coulomb electrode It is easy to calculate the damping Casimir energy,$W_{CASIMIR2}$, that appears between the intermediate position z_2 and the final position z_f .

We have the braking energy provided by $W_{CASIMIR2} = \int_{z_2}^{z_f} F_{CA}\,dz = \int_{z_2}^{z_f} S\ \frac{\pi^2\ \hbar\ c}{240\ z_s^4} dz_S = S\left(\frac{\pi^2\ \hbar\ c}{3*240}\right)\left[\frac{1}{z_f^3} - \frac{1}{z_2^3}\right]$ (Eq 31) We obtain :

$$W_{CIN1} - W_{ELECTRIC} = +\frac{1}{6}\,S\,\frac{\pi^2\ \hbar\ c}{240}\left(\frac{1}{z_2^3} - \frac{1}{z_f^3}\right) + \left(\frac{a_P}{2\ l_p b_P \epsilon_0\ \varepsilon_{PIEZO}}\right)\left(\frac{d_{31}\ l_p\ S\ \pi^2 c\ \hbar}{480\ a_P}\right)^2\left[\frac{1}{z_2^4} - \frac{1}{z_f^4}\right]^2 - \frac{1}{3}\,S\,\frac{\pi^2\ \hbar\ c}{240}\left(\frac{1}{z_2^3} - \frac{1}{z_f^3}\right)$$

This equation does not have an analytical solution to obtain zf but it is numerically solvable.

In a first approximation we observe that the term representing the ionic part WBRIDGE of the energy of the piezoelectric bridge,

$\left(\frac{a_P}{2\ l_{pbP}\epsilon_0\ \varepsilon_{PIEZO}}\right)\left(\frac{d_{31}\ l_p\ S\ \pi^2 c\ \hbar}{480\ a_P}\right)^2\left[\frac{1}{z_2^4}-\frac{1}{z_f^4}\right]^2$ is less than 0. 5% of the term in energy stored in the bridge through its deformation W_{DFCA}. So, to calculate the final arise of the loving system , we can approximate the kinetics' energy W_{CIN1} by the simplest approximate equation :

$W_{CIN1} - W_{ELECTRIC} = +\frac{1}{6}\ S\ \frac{\pi^2\ \hbar\ c}{240}\left(\frac{1}{z_2^3}-\frac{1}{z_f^3}\right)-\frac{1}{3}\ S\ \frac{\pi^2\ \hbar\ c}{240}\left(\frac{1}{z_2^3}-\frac{1}{z_f^3}\right)$. This equation gives the possibility to easily obtain an approximate value of z_f .

We deduce of this equation that the approximate final position z_f of the bridge is $z_f = \frac{1}{\sqrt[3]{\left[\frac{1}{z_2^3}\ \frac{1440\ (W_{CIN}-W_{ELECTRIC})}{S\ \pi^2\ \hbar\ c}\right]}}$ Eq 30 .

Note that this overall energy is represented by the kinetic energy W_{CIN1} acquired by the system.

Initially, we observe in Figure 20 that a minimum threshold voltage V_{T1mini} = 0.901V , is necessary for the final rising position z_f of the system to exceed the initial position z_0 .So an amplification $p_{mini} = F_{CO}/F_{CA}$ of about 100 (see Figure 15) is necessary to obtain that all the system return to its initial position or above .

Below this amplification threshold $p_{mini} = F_{CO}/F_{CA}$ of approximately 100, the final position z_f being lower than the initial position z_0, the system quickly stops after a few vibrations and becomes inoperative. For example , this is what happens if, a threshold voltage V_{T1} of 0.298 V is chosen so an amplification $p = F_{CO}/F_{CA}$ of about 23 (see Figure 15), starting from a position z_0 = 200 A°, the system only rises the position 198.9 A°, so 99% of its initial position (see Figure 20). Consequently, the device vibrates for approximately 460 vibrations before stopping completely.

Conversely, if we choose a threshold voltage V_{T1} greater than V_{T1mini}, for example V_{T1} = 1.51 V (therefore an amplification F_{CO}/F^{CA} = 225), then the system returns to the position z_f = 204.7 A°.

Consequently, as soon as the movement stops, the omnipresent Casimir force again deforms the piezoelectric bridge. The vibrations persist with the associated electrical power peaks.

Let us immediately clarify that we are in no way claiming to have invented an impossible perpetual motion or to have extracted energy from the vacuum. However, since the Casimir force arising from quantum vacuum fluctuations is continuously applied to the device supplying it with the necessary energy (not only the energy of the conservative Casimir Force) , it seems that this vibration could continue for a very long time.

To validate or invalidate this conclusion, a thorough study requiring significant resources - that a mere retiree cannot provide - is necessary.

We can see in Figure 20 that depending on the acquired inertia, which depends on the energy provided by the Coulomb force, zf can slightly exceed its initial position.

We will use this property at the end of this article in order to increase usable energy.(see Figure 28,29)

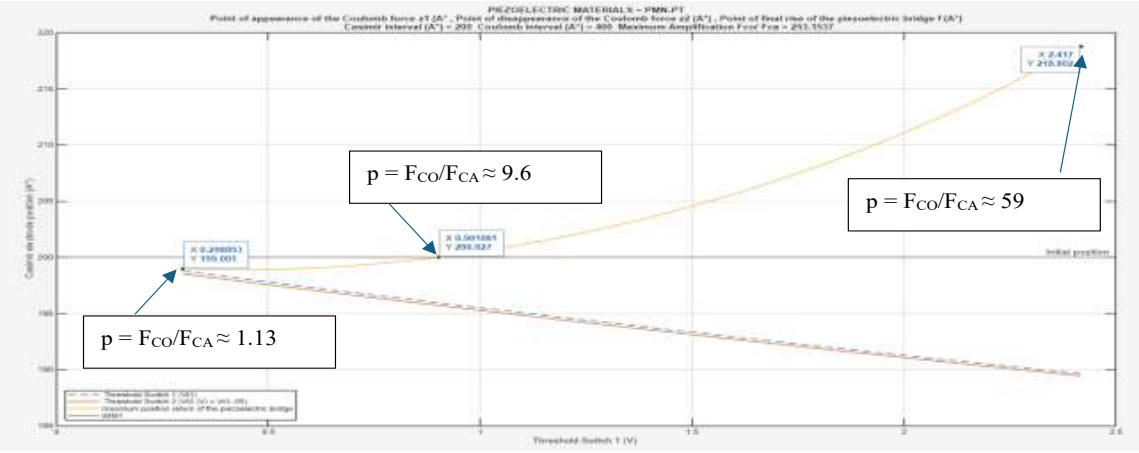

As, at position z_2 the switch n° 2 commutes to ON and puts the Coulomb electrode to ground through the RLC circuit below (Fig 21) the electrical charges present on the Coulombs electrode flow towards the ground, creating a current and a power which remains to be evaluated.

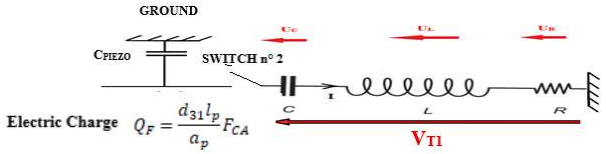

Figure 21 : RLC circuit to power the self-contained passive switching and rectification circuitry for

We now evaluate this usable current flowing to ground. We put in the circuit, an adjustment capacitance C in series with C_{PIEZO}. We call $C_E = \frac{C_{PIEZO}\, C}{C_{PIEZO} + C}$ the equivalent capacity of the two capacities in series. When the switch n°2 commutes, we have the equation $U_C + U_L + U_R = C_{PIEZO} / Q_F = V_{T1}$ (fig 21) , with : $U_R = R\, I$, $U_L = L\, dI/dt$ and $Q_F = V_{T1}\, C_{PIEZO}$.

R representing resistance, L inductance, and C capacitance.

After rearranging we have the following equation $\frac{d^2 U_C}{dt^2} + \frac{R}{L}\frac{dU_C}{dt} + \frac{U_C}{L\,C} = 0$ (Eq 32).

This differential equation has solutions that depend on the value of its determinant. We choose the values of R, L, C in such a way that the determinant $\Delta = \sqrt{\left(\frac{R}{L}\right)^2 - \frac{4}{LC}} = 0$ of this equation is positive or vanishes.

So, if $\Delta = 0$ the solution is : $x_1 = \frac{R}{2\,L}\left(-1 + \sqrt{1 - \frac{4\,L}{C\,R^2}}\right) = -\frac{R}{2\,L}$ and $x_2 = \frac{R}{2\,L}\left(-1 - \sqrt{1 - \frac{4\,L}{C\,R^2}}\right) = -\frac{R}{2\,L}$

then we have $x_1 = x_2 = -\frac{R}{2\,L}. < 0$ Considering the initial conditions, we obtain:

$$u_c = \frac{V_{T1}}{x_1 - x_2}\left[x_1 \exp(x_2 t) - x_2 \exp(x_1 t)\right] ,$$

$$i_c = C\frac{du_C}{dt} = C\frac{V_{T1}\; x_1 x_2}{x_1 - x_2}\left[\exp(x_2 t) - \exp(x_1 t)\right] \text{(Eq.33) .}$$

The peak of current is given when $d(i_c)/dt = 0$ so at the time $t_{imax} = \frac{Ln\left(\frac{x_2}{x_1}\right)}{x_1 - x_2} = \frac{Ln\left(\frac{1+\sqrt{1-\frac{4\,L}{C\,R^2}}}{1-\sqrt{1-\frac{4\,L}{C\,R^2}}}\right)}{\frac{R}{L}\sqrt{1-\frac{4\,L}{C\,R^2}}}$ (Eq .34).

Replacing t by t_{imax} in the equation 33 and 34 we obtain the expression for the maximum of the voltage is $u_{cmax} = V_{T1}$ and of the maximum current i_{cmax} ;

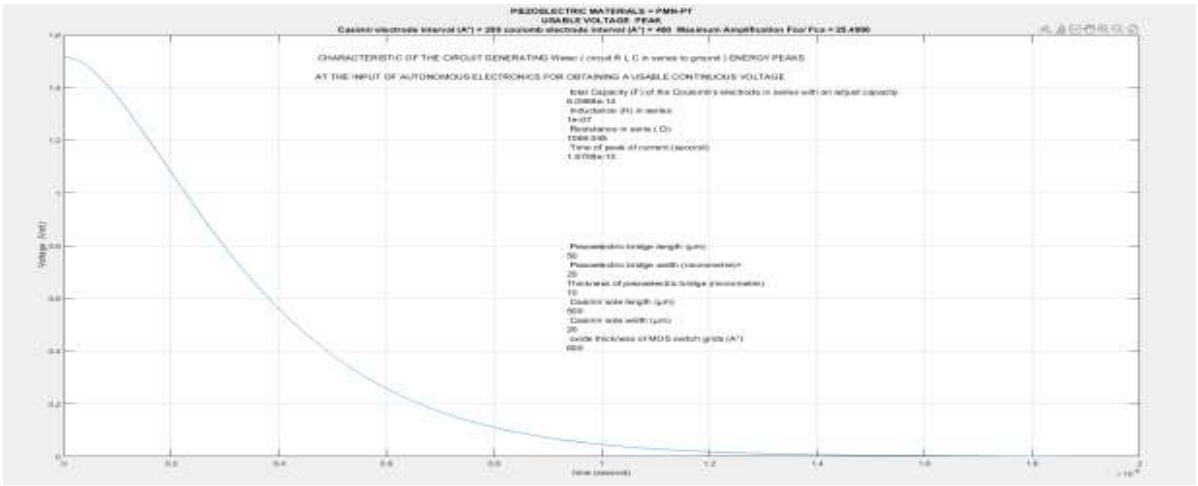

Figure 22 : Electric Voltage on the Capacitance C in Series with the Capacitance of the Coulomb Electrode

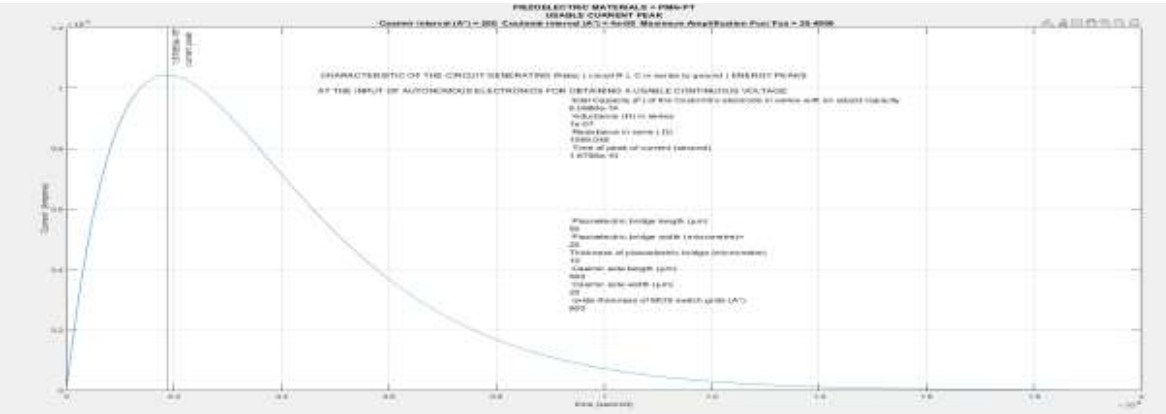

Figure 23: The Electric Current Flowing Through the Capacitance C in Series with the Capacitance of the Coulomb Electrode

We note on Fig 23 a maximum peak current of about 10^{-3} Ampere at time 2 10^{-10} seconde

The electrical power of the signal is :

$$P(t) = u_c\, i_c = \left(\frac{V_{T1}}{x_1 - x_2}\right)^2 C\, x_1 x_2\, [\exp(x_2 t) - \exp(x_1 t)][x_1 \exp(x_2 t) - x_2 \exp(x_1 t)] \quad \text{Eq35}$$

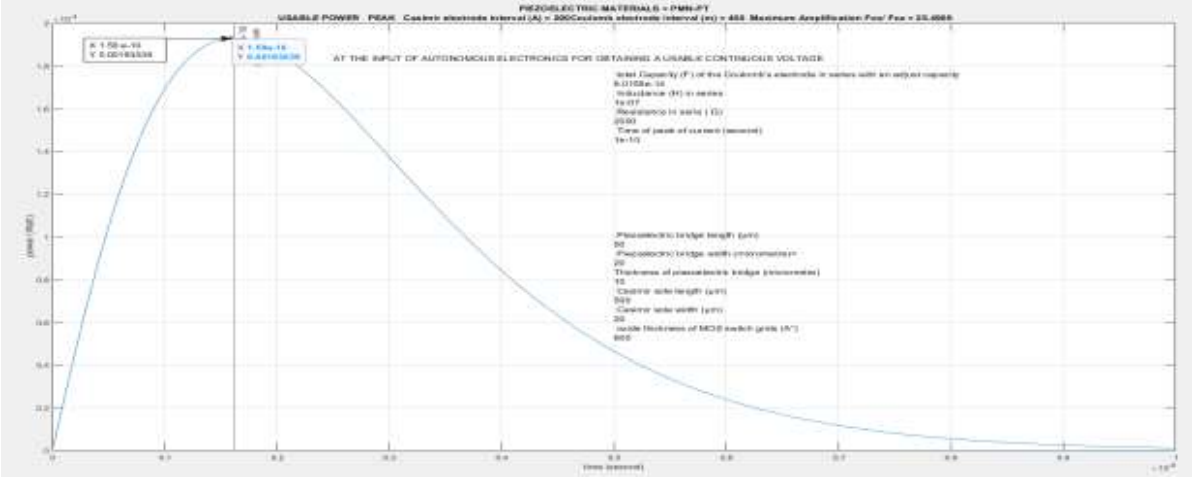

Figuer 24: Electrical Power of the Signal to Power the Self-Contained Passive Switching and Continuation

We note on Fig 23 and 24 that the maximum t_{imax} = 1.87 10^{-10} (s) for the peak current is different than those t_{pmax} = 3.03 10^{-10} for the peak power P(t) .

This peak power of 1.93 mW is sufficient to power the self-contained passive switching and rectification circuitry of fig 30,31 and obtain a useful voltage of several volts in a few milliseconds. The period of a vibration being (fig 10) of 0.2 µs for an F_{CO} /F_{CA} of simply 2, we calculate that the average power over a period is then approximately ≈ 0.3 µW.

Knowing the electrical power P(time) we can numerically evaluate by MATLAB the finale and useable energy $W_{ELECTRIC}$. We obtain $W_{ELECTRIC}$ in fig 27 . Since the electrical power P(time) drops rapidly, we approximate the energy $W_{ELECTRIC}$ between 0 and 10 t_{pmax}

$$W_{ELECTRIC}(t) = \int_0^{10 * tpmax} u_c\, i_c\, dt = \left(\frac{V_{T1}}{x_1 - x_2}\right)^2 C\, x_1 x_2 \int_0^{10 * tpmax} [\exp(x_2 t) - \exp(x_1 t)][x_1 \exp(x_2 t) - x_2 \exp(x_1 t)]\, dt \quad \text{(Eq.36)}$$

This value is easily calculable , so knowing $W_{ELECTRIC}$ energy balance we can calculate the "return" phase of the system to its initial position of the structure. The final position z_f of the system can be calculated saying that the effective W_{CIN1} who is used for the return of our system is $W_{CIN1FINAL}$ = W_{CIN} = W_{CIN1} - $W_{ELECTRIC}$ The energy consumes in the “returning” phase is :

Using this new value of the kinetic energy we obtain using the equation 30 the following figure for the final position z_f

$$\mathbf{W_{RETURNING1} = W_{CIN1} + W_{ELECTRIC} + W_{DFCA2} + W_{BRIDGE2} - W_{CASIMIR2} + \Delta Q_{vib}/2} \text{ (Eq. 37)}$$

With Figure 25, we can make the energy balance of the energy sources provided by the quantum vacuum in the "go" and "returning" phases. The energy provided by the quantum vacuum in the "go" phase is :

$$\mathbf{E_{VACUUM1} = W_{DFCA1} + W_{BRIDGE1} + W_{CASIMIR1} + \Delta\, Q_{vib1}/2} \text{ (Eq 24) .}$$

Note that we did not speculate from the start that $E_{VACUUM1} = W_{RETURNING1}$. We simply observe that the sum of the energy constituting the energy consumed during the "return" phase is practically the same as the total energy supplied by the vacuum.

These calculations can be improved because the calculated "return" energy is slightly less than the energy supplied. This can be explained by the failure to consider the energy associated with transistor switching and the approximations in this initial model. As Emmy Noether's theorem indicates, energy is indeed conserved. Simply the energy changes its nature and subdivides into other energies in the "return" phase of vibrations. One of these energies in this "return" phase can be used by creating a little electrical energy.

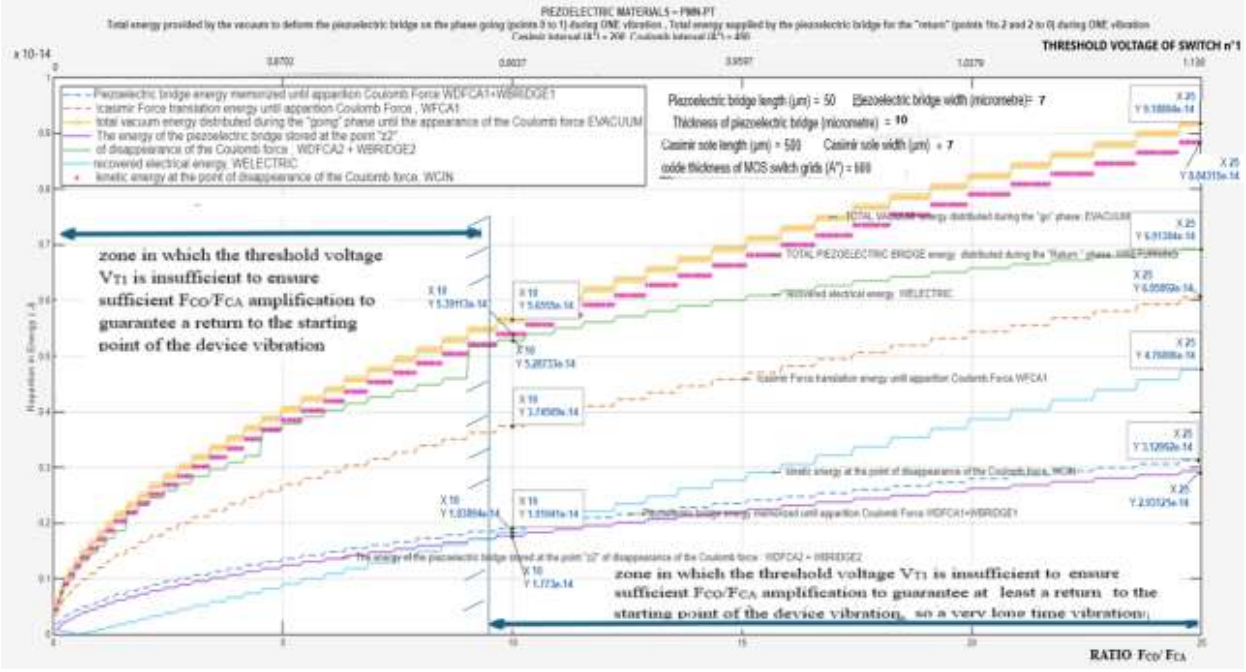

Figure 25: Balance of the Energies of the "go" and "return" Phases for the Proposed MEMS Which Seems to be able to "Extract Energy from the Quantum Vacuum."

We want to clarify an important point:
We do not assume, before any calculation, that $W_{RETURNING1} = E_{VACUUM1}$. However, we observe that if we calculate each component of the $E_{VACUUM1}$ energy expended by the vacuum during the phase from z_0 to z_1 of the system's vibration, and then each component of the $W_{RETURNING}$ energy during the return from z_1 to z_f of the vibrating system, then it clearly follows that $E_{VACUUM1} = W_{RETURNING1}$. In fact , $W_{RETURNING1}$ is very slightly lower (5%) than $E_{VACUUM1}$ due to the due to the neglect of the switching energy of the switches, which are assumed to be perfect, and the theoretical models used, which are first approximations.

Although Casimir's Force Is Conservative (which simply implies that its displacement energy between points z0 and z1 is equal on the way out and on the way back), **we show that there is no creation of energy but simply a report, by change of nature, of the** $E_{VACUUM1}$, energy brought by the vacuum during the first phase of the vibration from z0 to z1, into a WRETURNING1 energy during the return from z_0 to z_f.

This latter energy is dissipated in particular through the creation of electrical power peaks. These peaks are then stored and transformed into a direct current voltage usable by so-called autonomous electronics, that is, without any external power supply.

The energy expended by the vacuum ($E_{VACUUM1}$) is not simply the displacement energy (W_{FCA1}) of the Casimir force, but also the energy associated with the deformation of an elastic and piezoelectric bridge ($W_{DFCA1} + W_{BRIDGE1}$) , increased by the energy related to the entropy change expended as heat ($\Delta Qvib/2$).

Recall that: $E_{VACUUM1} = W_{DEFCA1} + W_{BRIDGE1} + W_{CASIMIR1} + \Delta QVIB/2$.

In this equation:

$W_{CASIMIR1} = W_{FCA1}$ = Translational energy of the Casimir force (F_{CA}) from the starting point z_0 to the point z_1 where the Coulomb force (F_{CO}) is triggered.

W_{DFCA1} = Mechanical deformation energy of the perfectly elastic bridge at point z_1.
$W_{BRIDGE1}$ = Electrical energy appearing at point z_1 in the deformation of an elastic and piezoelectric bridge.
ΔQ_{VIB} = Entropy change of the system appearing as heat during the vibration of the system from z_0 to z_1 and then from z_1 to z_f.
$W_{RETURNING1} = W_{CIN1} + W_{ELECTRIC} + W_{DFCA2} + W_{BRIDGE2} + \Delta Q_{VIB}/2 - W_{CASIMIR2}$ With:
W_{CIN1} = Kinetic energy of the entire structure (piezoelectric bridge + Casimir moving electrode)
$W_{CIN1} = [(W_{DFCA1} + W_{BRIDGE1}) - (W_{DFCA2} + W_{BRIDGE2})] + W_{COULOMB} - (W_{CASIMIR1} - W_{CASIMIR2})$

Recall the mathematical expression of these energies :

The Casimir' Force = $F_{CA} = S_s \frac{\pi^2 \hbar c}{240 z_s^4}$ (Eq. 1)

The electrical charge on the piezoelectric bridge : $Q_F = \frac{d_{31} l_p}{a_p} F_{CA} \Rightarrow Q_F = \frac{d_{31} l_p}{a_p} S_s \frac{\pi^2 \hbar c}{240} \left(\frac{1}{z_s^4} - \frac{1}{z_0^4}\right)$(Eq. 2)

The Coulomb's Force $F_{CO} = \frac{Q_p^2}{4\pi\epsilon_0\epsilon_r}\left(\frac{1}{z_r + z_0 - z_s}\right)^2 = \left[\frac{d_{31} l_p}{a_p} S_s \frac{\pi^2 \hbar c}{240}\left(\frac{1}{z_s^4} - \frac{1}{z_0^4}\right)\right]^2 \left(\frac{1}{8\pi\epsilon_0\epsilon_r}\right)\left(\frac{1}{z_r + z_0 - z_s}\right)^2$ (Eq. 5)

$W_{CASIMIR1} = W_{FCA1} = W_{CASIMIR1} = \int_{z_0}^{z_1} F_{CA}\, dz = \int_{z_0}^{z_1} S \frac{\pi^2 \hbar c}{240 z_s^4} dz_S = S\left(\frac{\pi^2 \hbar c}{720}\right)\left[\frac{1}{z_1^3} - \frac{1}{z_0^3}\right]$(Eq 18)

$W_{CASIMIR2} = W_{FCA2} = W_{CASIMIR2} = \int_{z_1}^{z_f} F_{CA}\, dz = \int_{z_1}^{f_1} S \frac{\pi^2 \hbar c}{240 z_s^4} dz_S = S\left(\frac{\pi^2 \hbar c}{720}\right)\left[\frac{1}{z_1^3} - \frac{1}{z_f^3}\right]$

The position z_1 of appearance of the Coulomb's force F_{CO} is such that $F_{CO} = p F_{CA}$ and is numerically calculated by MATLAB (fig. 18) by solving numerically the equation :

$F_{CO} = pF_{CA} \Rightarrow \frac{Q_F Q_F}{8\pi\varepsilon_0\varepsilon_r}\left(\frac{1}{z_r + z_0 - z_S}\right)^2 = \left[\frac{d_{31} l_p}{a_p} S_S \frac{\pi^2 c \hbar}{240}\left(\frac{1}{z_S^4} - \frac{1}{z_0^4}\right)\right]^2 \left(\frac{1}{8\pi\varepsilon_0\varepsilon_r}\right)\left(\frac{1}{z_r + z_0 - z_S}\right)^2 = p S \frac{\pi^2 c \hbar}{240 z_S^4}$ (Eq 25).

The final position of the Casimir mobile electrode $z_f = \frac{1}{\sqrt[3]{\left[\frac{1}{z_2^3} - \frac{1440 W_{CIN}}{S \pi^2 \hbar c}\right]}}$ Eq 30 .

The point of disappeared of the Coulomb' force $z_2 = \frac{1}{\sqrt[4]{\left[\frac{240 a_p C_{ox}}{d_{31} l_p \pi^2 c \hbar S_S} V_{T2} + \frac{1}{z_0^4}\right]}}$ Eq 27

$W_{CIN1} = [(W_{DFCA1} + W_{BRIDGE1}) - (W_{DFCA2} + W_{BRIDGE2})] + W_{COULOMB} - (W_{CASIMIR1} - W_{CASIMIR2})$ (Eq. 28) and fig 20

$$W_{CIN1} = +\frac{1}{6} S \frac{\pi^2 \hbar c}{240}\left(\frac{1}{z_2^3} - \frac{1}{z_f^3}\right) + \left(\frac{a_P}{2\ l_P b_P \epsilon_0\ \varepsilon_{PIEZO}}\right)\left(\frac{d_{31}\ l_p\ S\ \pi^2 c\ \hbar}{480\ a_P}\right)^2 \left[\frac{1}{z_2^4} - \frac{1}{z_f^4}\right]^2 - \frac{1}{3} S \frac{\pi^2 \hbar c}{240}\left(\frac{1}{z_2^3} - \frac{1}{z_f^3}\right)$$

$$W_{DFCA1} = \frac{1}{2} S \frac{\pi^2 \hbar c}{720}\left[\frac{1}{z_1^3} - \frac{1}{z_0^3}\right] \text{ Eq. 20,} \quad W_{DFCA2} = \frac{1}{2} S \frac{\pi^2 \hbar c}{720}\left[\frac{1}{z_2^3} - \frac{1}{z_0^3}\right] \text{Eq.21}$$

$$W_{BRIDGE1} = \int_0^{Q_1} Q_F\, d(V_{PIEZO}) = \int_0^{Q_1} \frac{Q_F}{C_{PIEZO}}\, d(Q_F) = \left[\frac{Q_F^2}{2\ C_{PIEZO}}\right]_0^{Q_1} = \frac{a_P}{2\ l_P b_P \epsilon_0\ \varepsilon_{PIEZO}}\left(\frac{d_{31}\ l_p}{2\ a_P}\right)^2 F_{CA}^2 =$$

$$\left(\frac{a_P}{2\ l_P b_P \epsilon_0\ \varepsilon_{PIEZO}}\right)\left(\frac{d_{31}\ l_p\ l_s b_s\ \pi^2 c\ \hbar}{480\ a_P}\right)^2 \left[\frac{1}{z_1^4} - \frac{1}{z_0^4}\right]^2 \qquad \text{Eq. (22)}$$

$$W_{BRIDGE2} = \left(\frac{a_P}{2\ l_P b_P \epsilon_0\ \varepsilon_{PIEZO}}\right)\left(\frac{d_{31}\ l_p\ l_s b_s\ \pi^2 c\ \hbar}{480\ a_P}\right)^2 \left[\frac{1}{z_2^4} - \frac{1}{z_0^4}\right]^2$$

$$W_{COULOMB} = \int_{z_2}^{z_1} F_{C0}\, dz = \left\{S_S \cdot \frac{\pi^2 \hbar c}{240} \cdot \frac{d_{31}\ l_p}{a_p}\right\}^2 \left(\frac{1}{8\,\pi\epsilon_0\ \epsilon_r}\right) \cdot \int_{z_2}^{z_1} \left[\left(\frac{1}{z_s{}^4} - \frac{1}{z_0{}^4}\right)\left(\frac{1}{z_r + z_0 - z_s}\right)\right]^2 dz_s \text{ Eq.26}$$

$$W_{ELECTRIC}(t) = \int_0^{10*\,tpmax} u_c\, i_c\, dt = \left(\frac{V_{T1}}{x_1 - x_2}\right)^2 C\, x_1 x_2 \int_0^{10*\,tpmax} [\exp(x_2 t) - \exp(x_1 t)][x_1 \exp(x_2 t) - x_2 \exp(x_1 t)]\, dt \text{ (Eq.36)}$$

$$x_1 = \frac{R}{2\,L}\left(-1 + \sqrt{1 - \frac{4\,L}{C\,R^2}}\right) = -\frac{R}{2\,L} \text{ and } x_2 = \frac{R}{2\,L}\left(-1 - \sqrt{1 - \frac{4\,L}{C\,R^2}}\right) = -\frac{R}{2\,L}$$

We note that these amplifications assume that the final rise zf of the moving Casimir electrode is greater than zo, so that the vibration must persist over time.

We note that the energy necessary for the perpetual maintenance of these vibrations is constantly provided by the isotropic and timeless energy of the quantum vacuum. Regardless of the F_{CO} / F_{CA} amplification factor, we find that $W_{RETURNING1}$ is always slightly lower than $E_{VACUUM1}$, despite the use of $W_{ELECTRIC}$ electrical energy. The fact that the $W_{RETURNING1}$ energy is slightly lower than the energy supplied $E_{VACUUM1}$ for all F_{CO} / F_{CA} ratios can be explained by :

1/ the neglect of the energy used for the switching of the TFT MOS transistors,
2/ the approximation of the simplified models used,
3/ by the fact that we considered the piezoelectric bridge to be perfectly elastic... but note that the difference is very small and represents only a maximum of 3.8% for a ratio of 23.6 (fig 25).

An important Key Clarification: is it is NOT an Energy Extraction from the vacuum but an Energy Conversion !

The proposed NEMS system does not extract energy. Instead, it converts mechanical energy—originating from the deformation of the piezoelectric bridge induced by the Casimir force—into electrical energy. The quantum vacuum fluctuations provide a conservative mechanical force, while the actual energy conversion relies on the transient Coulomb interaction and piezoelectric effect. This process fully complies with the laws of thermodynamics and Noether's theorem on energy conservation.

So , we are allowed to say that in the referential of our 4 dimensions Space-Time plus the Quantic Vacuum, the energy is conserved . This is consistent with Noether's theorem.This very important theorem of 1905 explains why, as Monsieur de Lavoisier said, "Nothing is created, nothing is lost, everything is transformed." .

Remember also that energy is defined as the physical quantity that is conserved during any transformation of an isolated system. However, the system constituted by simply the MEMS device in time-space is not really an isolated system while the system constituted by the MEMS device in the time-space plus the energy vacuum seems an isolated system.

As the part of the MEMS energy sensor vibrates at frequencies - depending on the size of the structure and operating conditions- but with an amplitude of just a few Angstroms, these vibrations do not constitute a perpetual motion since they can be continuously powered by the energy of the vacuum generating the Casimir force.

The shape of the electrical energy peaks generated by the system is shown in Figure 25.

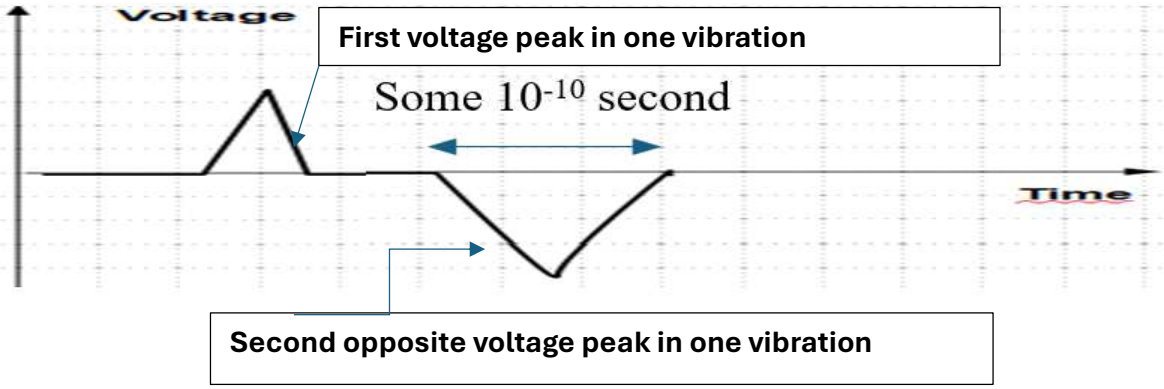

Figure 25: Shape of the Electrical Energy Peaks Generated by One Piezoelectric Bridge System

The following diagram summarizes the operation of this presented MEMS (Figure 26 and 27).

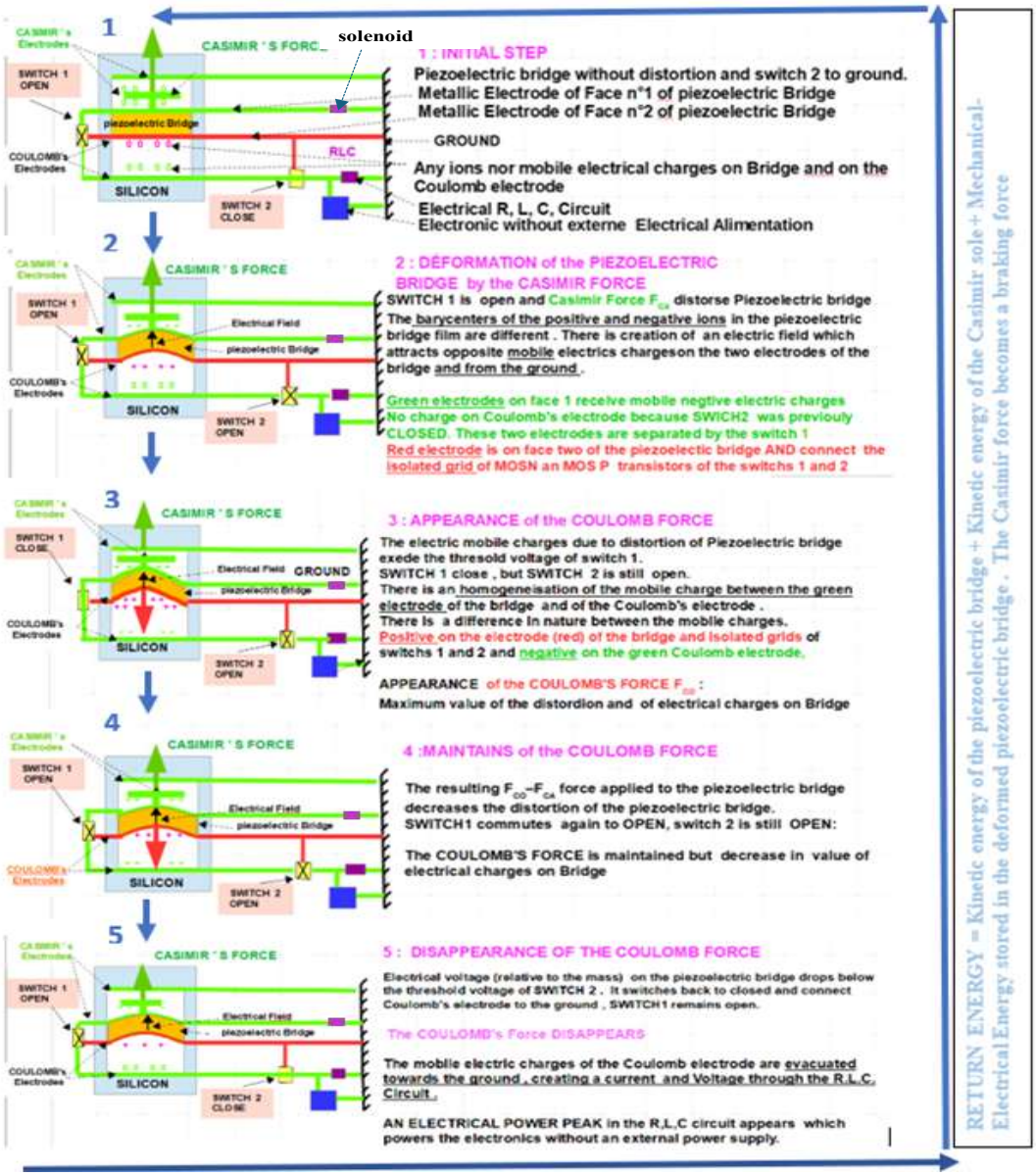

Figure 26: Overview of the 5 Successive and Repetitive Steps of the M.E.M.S

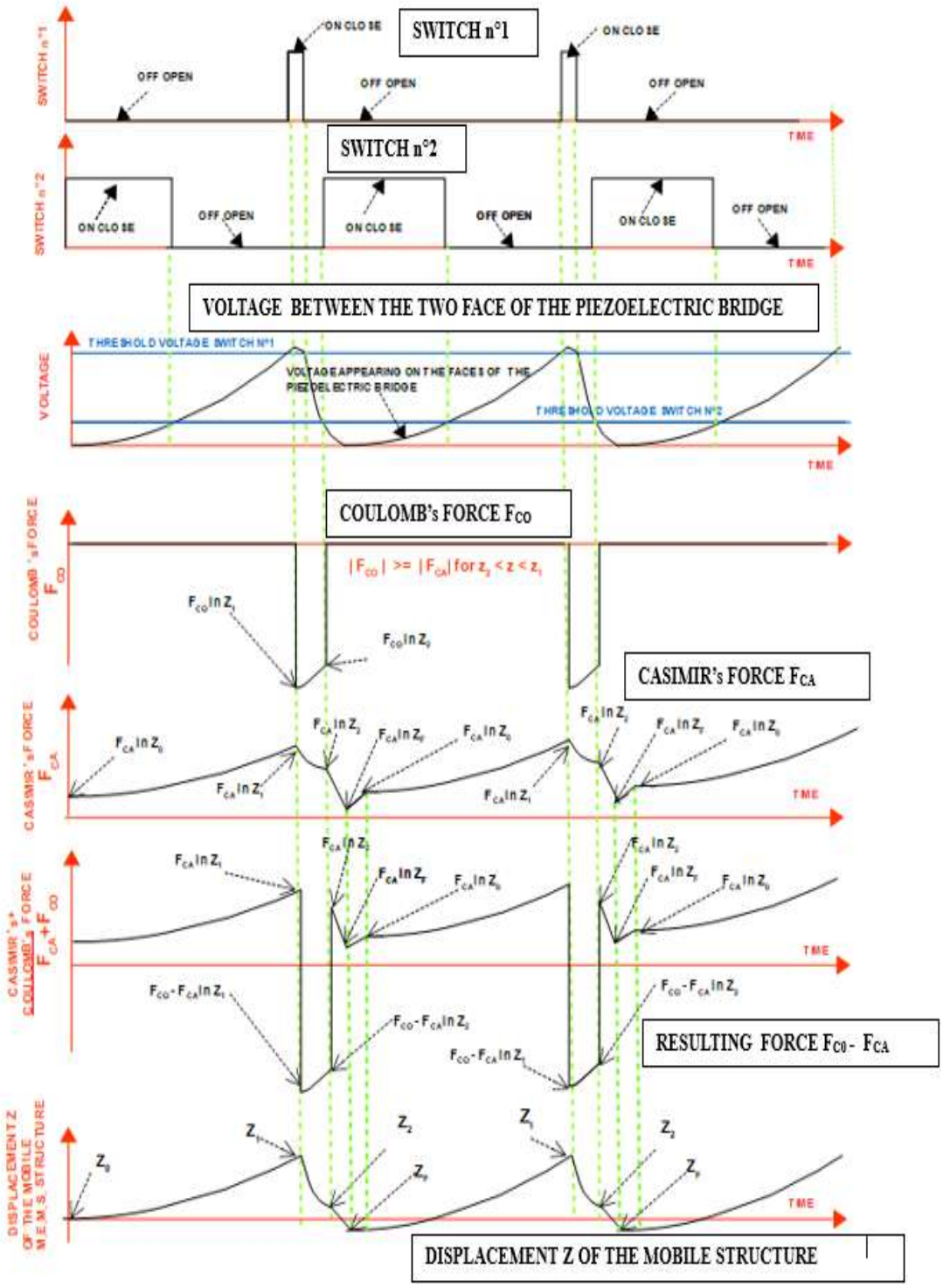

Figure 27: Shape of the Curves Representing 1/ The switching of the Two Switches 2/ The Electrical Voltage on Face 1 of the Piezoelectric Bridge 3/ The Casimir Forces F_{CA} 4/ The Coulomb Forces F_{CO} 5/ the Energies W_{FCO}, W_{FCA} , W_{FCO} -W_{FCA} 6/ The Maximum Elevation zf of the Moving Part

We notice in the previous pages that the piezoelectric bridge could reach a position zf which exceeds its initial position z_0.

We can take advantage of this observation by modifying the moving part of this MEMS to provide the RLC circuit with the two signs of current peak and voltage emitted by the sensor. This modification should increase the continuous electrical voltage on the capacitive

output of the autonomous electronic circuit whose role is to transform the signals from the quantum vacuum energy sensor(fig 28). The inconvenience of this proposal is that it greatly increases the inertia of the structure and therefore significantly decreases the frequency of vibrations of the structure

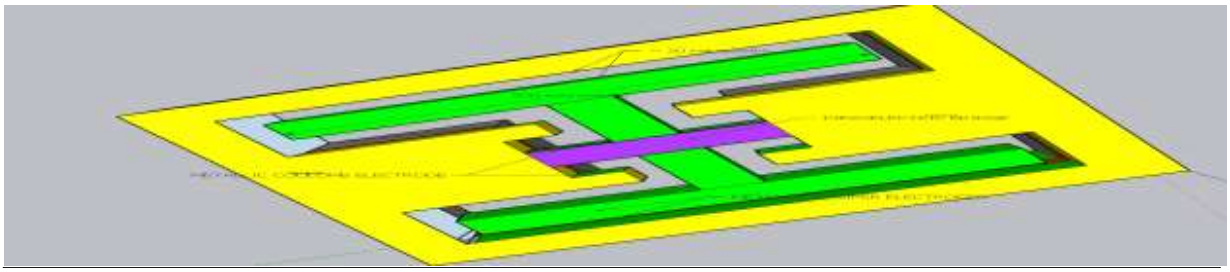

Figure 28: Shape of the MEMS Circuit Making it Possible to Double the Direct Voltage at the Output of the Autonomous Electronic Circuit, by Providing it with Consecutive Voltage and Current Peaks of Opposite Sign

In the following figure 29 , we arranged the Casimir electrode on the other side of its piezioelectric bridge. Consequently, the charges drawn back and then removed from the Coulomb electrode will be opposite to those in the previous situation. The voltage peak supplying the self-contained passive switching and rectification circuitry will therefore also be opposite. This electronic will convert these two repeating and opposing peaks voltage into two DC voltages: one positive and the other negative with respect to ground.

To avoid that the two opposite peaks overlap, so they cancel each other, they must be offset. For this, simply modify the value, for example, of the self of the RLC2 circuits compared to the self of the RLC1 circuits since the maximum of the peaks occurs at time

$$t_{imax} = \frac{Ln\left(\frac{x_2}{x_1}\right)}{x_1 - x_2} = \frac{Ln\left(\frac{1+\sqrt{1-\frac{4L}{CR^2}}}{1-\sqrt{1-\frac{4L}{CR^2}}}\right)}{\frac{R}{L}\sqrt{1-\frac{4L}{CR^2}}} \quad \text{(Eq 34)}$$

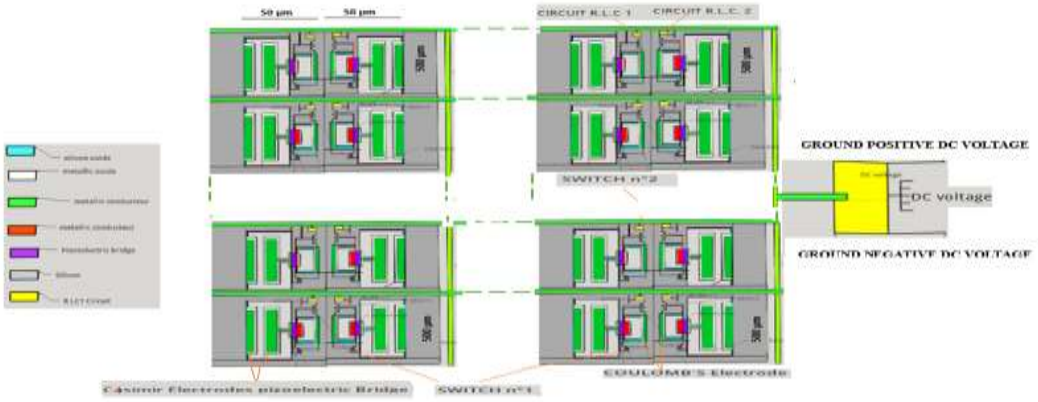

Figure 29: Positioning of 50 Casimir Cells in Parallel and 10 in Series. Total of Casimir Cells Delivering a Periodic Current During a Small Part of the Vibration Frequency of the Devices = 50 . Total Number = 200, Width = 5mm, Length = 6 mm

In order to increase the peak current intensity, the Casimir cells may be interconnected in combined series–parallel networks, enabling the power supply of a single autonomous electronic module that converts the voltage and current peaks produced by the RLC circuits into a direct voltage. As depicted in figure 29, for example, 50 Casimir cells can be placed in parallel and 10 in series so that about 500 devices (approximately 5*6 mm^2 area) send their signal to one self-contained passive switching and rectification circuitry transforming the different voltage and current peaks into a DC voltage (Figure 29). The objective is, of course, to increase the energy stored on the capacitive system at the end of the self-contained passive switching and rectification circuitry that transform the power peaks generated by the system.

5. Passive Autonomous Switching Electronics to Transform the Cyclic Power Peaks From the R.L.C. Circuit

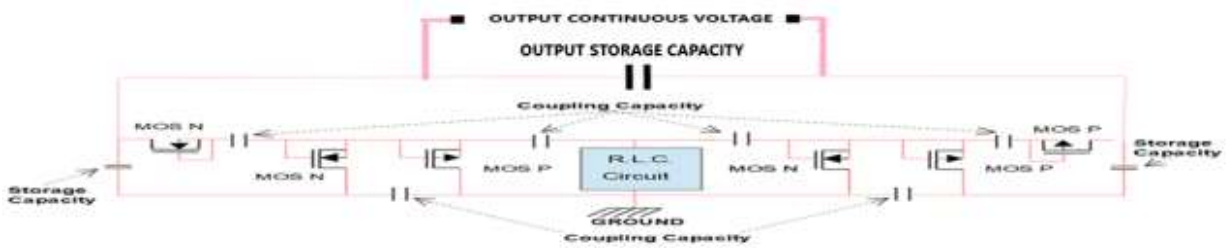

Figure 30: Principle of the Single-stage Doubler Without Power Supply Electrical Diagram. All the MOS are Isolated From Each Other by Etching on an S.O.I Wafer, and Their Threshold Voltage is as Close as Possible to Ground

The circuit of the figure 30 is an autonomous device operating without any electrical power source. It rectifies and accumulates the repetitive peak power delivered to the terminals of the RLC circuit in the figure 1 and 2 and transforms them into a usable direct voltage source. The impedance of the output of this autonomous circuit must be important. The results provided by these self-contained passive switching and rectification circuitry are illustrated in the figure 31

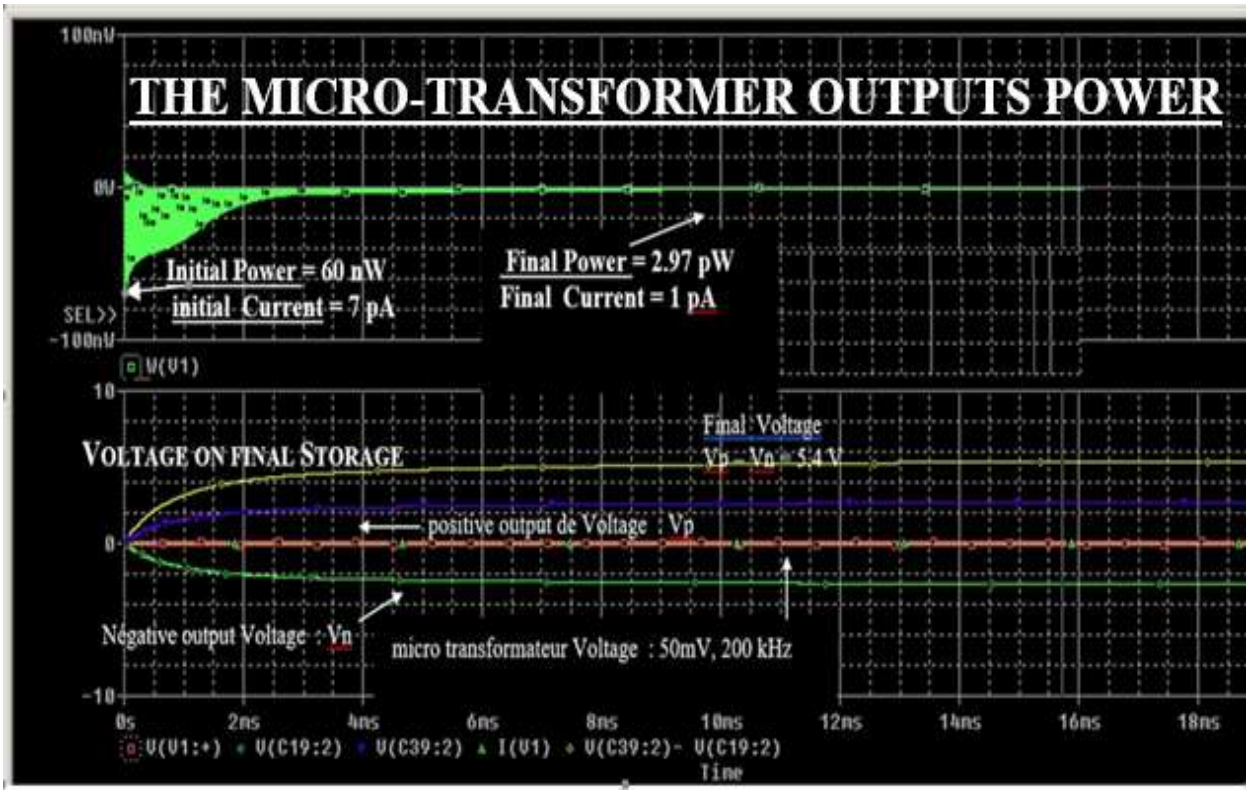

Figure 31: SPICE Simulations of Voltages, Current, Power Consumed by the Self-contained Passive Switching and Rectification Circuitry for the Transformation into Direct Voltage (5.4 V) of an Alternating Input Signal of 50 mV, Frequency = 150 kHz, Number of stages = 14, Coupling Capacities = 20 pF, Storage Capacity = 10 nF

We note the extreme weakness of the electrical power required at the start of the conversion of the power peaks (60 nW) and at the end (2 pW). The conclusions are the same for the electrical current consumption of the transformation electronics, both at the beginning of the transformation (9 pA) and at the end (2 pA). This electrical consumption is significantly lower than what the RLC source can supply. The transformation of the peak of power of 150 kHz , requires about 4 ms.

The interesting points for this presented electronics device are for this SPICE simulation :
1 / the low alternative (50 mV) input voltages required to obtain a continuous voltage of several volts at the output
2 / the low power and low current consumed by the source, which in this case is only an RLC circuit, powered by current spikes

generated by autonomous vibrations, for this conversion and amplification circuit.
3 / the rapid time to reach the DC voltage (a few ten milliseconds)
The technology used to fabricate the MOSNE and MOSPE transistors of this autonomous electronic, which have the lowest possible threshold voltages, is CMOS on intrinsic S.O.I. and each element is isolated from each other on independent islands. This technology, represented in the following figure 31, strongly limits the leakage currents.

To create these self-contained passive switching and rectification circuitry, we propose using CMOS technology on intrinsic SOI, which isolates each element from the others, thus greatly limiting leakage currents.

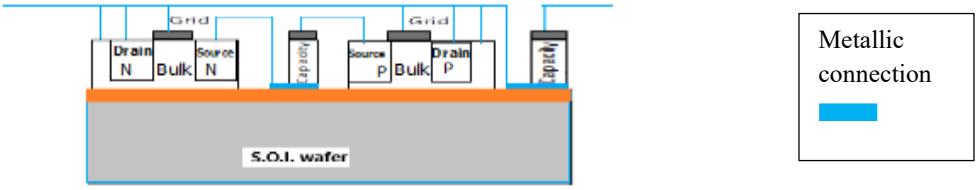

Figure 31: S.O.I Technology for Making the Elements of the "Doubler"

CHARACTERISTICS OF OUTPUT VOLTAGES (V), POWERS (nW) CURRENTS (nA)
AS A FUNCTION OF THE NUMBER OF STAGES
INPUT SIGNAL FREQUENCY = 150 kHz OUTPUT VOLTAGE MEASUREMENT FOR t = 50 ms

	Vg=50mV					Vg=100mV				
number of stages	Output Voltage	Current (nA) start	Current (nA) end	Power (nW) start	Power (nW) end	Output Voltage	Current (nA) start	Current (nA) end	Power (nW) start	Power (nW) end
2*3	550mV	300nA	26nA	15nW	1.3nW	1.1v	800nA	46nA	75nW	5nW
2*6	1	300nA	29nA	13nW	1.3nW	2V	700nA	67nA	60nW	6.5nW
2*14	2.2v	300nA	40nA	14nW	2.6nW	4.5v	700nA	50nA	65nW	4.8nW
2*21	2.8v	250nA	38nA	13nW	860pw	6v	600nA	80nA	60nW	2.7nW
2*30	3.3	250nA	43nA	12nW	1.2nW	6.5V	750nA	85nA	61nW	4nW
2*39	3.5v	250nA	45nA	12nW	900pW	7.5V	750nA	95nA	64nW	3.5nW
2*48	3.6v	250nA	46nA	12nW	1nW	7.6V	750nA	100nA	60nW	4.2nW
2*60	3.8	270nA	47nA	12nW	1.1nW	7.9V	700nA	90nA	65nW	4.2nW
2*61	3.8	270nA	48nA	12.1nW	1.3nW	8V	700nA	90nA	65nW	42nW

Figure 32: Table 1, Output Continuous Voltage , with Current and Power Consumed by the Autonomous Electronic in Function of Two Input Cyclic Voltage Parametrized with the Number of Stages

We note that the coupling capacities of 20 pF of this electronic, like that of storage of the order of 10 nF, have relatively high values. To minimize the size of these capacitors we propose to use of titanium dioxide as insulator, with a relative permittivity of the order of 100 which is one of the most important for a metal oxide, then the size of the capacity passes to 33 µm for a thickness of TiO2 = 500 Å, which is more reasonable

6. Technology of Realization of the Current Extractor Device Using the Forces of Casimir in a Vacuum

For the structures presented above, the space between the two surfaces of the reflectors must be of the order of 200 Å, ... which is not technologically feasible by simply engraving. It seems possible, however, to obtain this parallel space of approximately 200 Å between the Casimir reflectors, not by chemical etching, but by thermal growth or, preferably, by Atomic Layer Deposition (ALD).
Indeed, the Ss3 and Ss2 surfaces of the Casimir reflector must (figure 1 ,2) :
• be metallic to conduct the mobile charges
• insulating as stipulated by the expression of Casimir's law who established for surfaces without charges.
• This should be possible if we grow an insulator on the z direction of the structure, for example Al_2O_3 or TiO_2 or other oxide metal which is previously deposited and in considering the differences in molar mass between the oxides and the original materials.

For example, silicon has a molar mass of 28 g/mol and silicon dioxide SiO2 of 60 g/mol. It is well known that when silicon dioxide SiO2

grows by one unit, a silicon depth of about 28/60 = 46.6%. This means that the fraction of oxide thickness "below" the initial surface is 46% of the total oxide thickness according to S.M. Sze. [9]

The same must happen, for example for thermal growth of alumina. The molecular masses of Alumina and aluminum are MAl_2O_3 = 102 g/mole and MAl = 27 g/mole. We obtain an aluminum attack ratio of 27/102 = 26%, which implies that the original surface of this metal has shifted by 26% so that 74% of the alumina has grown out of the initial surface of the aluminum....

As regards the technological manufacture of electronics and structure, it therefore seems preferable:
1 / For electronics to choose Titanium Oxide because of its high relative permittivity εr =114 allowing to minimize the geometries required for the different capacities
2 / For the Casimir structure, the choice of aluminum, because its low density increases the resonant frequency of the structure and that 74% of the Alumina Al_2O_3 is outside the metal, allowing to reduce the interface between Casimir electrodes. A simple calculation shows for example that for aluminum gives...:

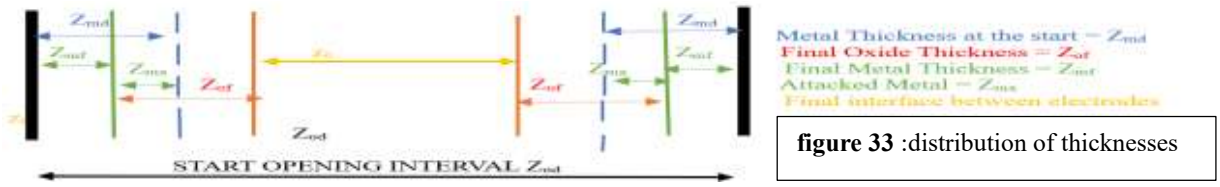

figure 33 :distribution of thicknesses

$$z_{od} = 2(z_{md} + z_{of} - z_{ma}) + z_o = 2[z_{md} + (1-0.26)\, z_{of}] + z_o \Rightarrow z = z_{od} - 2\left(z_{md} + 0.74\, z_{of}\right).$$

If thermal oxidation is used rather the preferred Atomic Layer Deposition, then :

For example, after an opening Zod = 3 µm. We deposit a metal layer of aluminum that is etched leaving a width z_{md} = 1 µm on each side of the reflector. We then grow a layer of alumina Al_2O_3 whose thickness is precisely adjusted, simply by considering time, temperature and pressure, in order to obtain the thickness necessary to have the desired z_0 interface. For example, if z_0 = 200 Å, Z_{od} = 3 µm, z_{md} = 1 µm, then the grow of AL_2O_3 on the 1µm of Aluminum is z_{of} = 0.662 µm .The final metallic layer Al remaining will be z_{mf} = 0.338 µm and will act as a conductor under the aluminum oxide.of about 400 A° . So, we obtain a Casimir interface of 200 Å.

Obviously, the growth of this metal oxide between the electrodes of the Casimir reflector modifies the composition of the dielectric present between these electrodes, therefore of the mean relative permittivity of the dielectric. Let: ε0 be the permittivity of vacuum and ε_0. εr the metal oxides one (ε_r = relative permittivity ≈ 8 in the case of Al_2O_3), z_{of} the final oxide thickness on one of the electrodes and z the thickness of the vacuum present between electrode, (initially we want z = z_0).

Figure 34: Material Repartition Between the Vacuum z0 Space

Then the average permittivity ε_{0m} of the dielectric is:

$\varepsilon_{0m} = (z_{of}\, \varepsilon_0\, \varepsilon_r + z_0\, \varepsilon_0 + z_{of}\, \varepsilon_0\, \varepsilon_r) / (2\, z_{of} + z_0) = \varepsilon_0\, (2z_{of}\, \varepsilon_r + z_0) / (2z_{of} + z_0) \approx \varepsilon_0\, \varepsilon_r$, because z_0 is << z_{of}...

For example, z_{of} = 6620 Å is large compared to z << 200 Å therefore $\varepsilon_{0m} \approx 8 \times \varepsilon 0$ in the case of Al_2O^3.

We have considered this change in permittivity in the preceding simulations.

7. Steps For the Realization of the Structure and its Electronics

We use an SOI wafer with an intrinsic silicon layer : The realization start with voltage "doubler" is obtained by using CMOS technology with 8 ion implantations on an SOI wafer to make :

1. The sources, drains of the MOSNE, MOSND of the "doubler" and of the Coulomb force trigger circuits and of the grounding
2. The source, drains of the MOSPE, MOSPD of the "doubler" and of the Coulomb force trigger circuits

3. Optimally adjust the zero-threshold voltage of the MOSNE in the "doubler" circuit.
4. Optimally adjust the zero-threshold voltage of the MOSPE in the "doubler" circuit.
5. To define the threshold voltage of the MOSNE of the circuit n°1
6. To define the threshold voltage of the MOSPE of the circuit n°1
7. To define the threshold voltage of the MOSND of the circuit n°2
8. To define the MOSPD threshold voltage of the circuit n°2

This electronic done, we take care of the vibrating structure of CASIMIR by :
9. engrave the S.O.I. silicon to the oxide to define the location of the Casimir structures (figure 35)

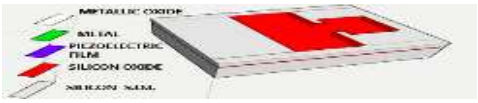

Figure 35: 9. etching of S.O.I

10. Place and engrave a protective metal film on the rear faces of the S.O.I wafer (figure 36)

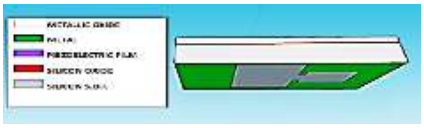

Figure 36: 10. Engraving of the Protective Metal Rear Face of the S.O.I. Silicon

11. Deposit and engrave the piezoelectric layer (figure 37)

Figure 37: 11. Deposition and Etching of the Piezoelectric Layer Deposition and Etching

12. Depose and etch the metal layer of aluminum (Figure 38).

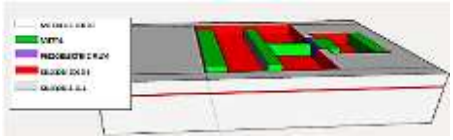

Figure 38: 12. Metal Deposit, Metal Engraving Etching of the Piezoelectric Layer

13. Plasma etching on the rear side the silicon of the Bulk and the oxide of the S.O.I wafer protected by the metal film to free the Casimir structure then very finely clean both sides (figure 39)

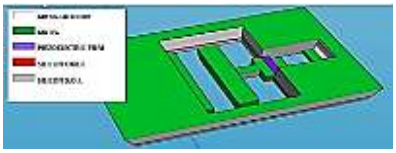

Figure 39: 13. view of the Casimir Device on the Rear Face, Engraving on the Rear Face of the Structures

14. After extremely careful cleaning and cutting of the wafer obtained , place the structure in a hermetic integrated circuit support box and carry out all the bonding necessary for the structure to function. After having put the structure in a final box , proceed to the last oxidation under a temperature lower than 150°C of the entire MEMS or preferably by an Atomic Layer Deposition (ALD) . The thickness of the ALD layer is extremely homogeneous, and ALD deposition is considered perfectly conformal. Under ideal temperature and pressure conditions, with properly chosen parameters, the chemical reactions are complete, thus leaving no impurities in the coating. The coating is dense and exhibits homogeneous, non-columnar growth . The objective is to obtain an adequate Casimir's and Coulomb's interface , which is given by the measurement of a adequate voltage obtained at the output of the autonomous transformation electronics.

The in situ electronic circuit should generate a automatic and measurable electrical signal when the interface between the Casimir electrodes becomes weak enough for the device to vibrate and generate a DC voltage, thereby stopping oxidation or ALD deposition.

This voltage measurement indicates that the Casimir and Coulomb effect are effective and automatically controls the end of the oxidation or ALD.

Then the box is closed under neutral gas or vacuum.

This thermal oxidation or ALD after very fine cleaning of the wafer and at the very end of the process makes it possible to control the thickness of the very fine interface between the Casimir and Coulomb electrodes and to oxidize the cleanest possible surfaces without defects.

We obtain the device of (Figure 40)

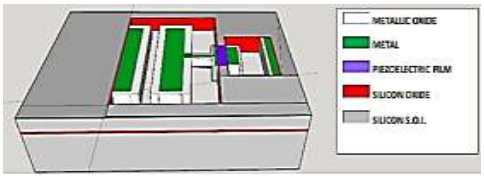

Figure 40: 14. Adjusted Growth of Metal Oxide Front View of the Casimir Device and Coulomb's Electrode, Under Automatic Electronic Control.

15. Create a neutral ambiance or better a vacuum in the hermetic box

We remark also that in the case where the 2 metal electrodes of Casimir adhere to one another, they can be separated by the application of an electrical voltage on Coulomb's electrodes.

8. Conclusion and Future Perspectives

This work analyzes a nonlinear electromechanical system combining Casimir interactions, elastic deformation, and piezoelectric charge generation within a fully conservative theoretical framework. The proposed model demonstrates that a measurable electrical signal can be generated without any classical external power supply, through the internal redistribution of energy associated with the system's configuration, including Casimir-dependent boundary conditions.

Part of these repetitive electrical power spikes powers an electronic circuit without any other external power source. The other part is converted into a direct current voltage that evolves in a few milliseconds to a usable voltage of a few volts. The energy consumption of this electronic circuit on these repetitive power peaks is very low.

The Casimir interaction is treated as a configuration-dependent potential energy, constituting an intrinsic part of the system's total Hamiltonian. Variations in this energy, induced by controlled geometric deformation, are redistributed into elastic energy, electrostatic energy, kinetic energy, and dissipative losses, in perfect conformance with the principles of energy conservation and time translation invariance.

No net extraction of energy from the quantum vacuum is claimed. The device is not a self-contained energy source, but rather a nonlinear energy converter capable of transforming internal configuration energy into transient electrical signals. All generated electrical energy is compensated by the corresponding losses, including electromechanical dissipation and electronic imperfections.

It should be noted that an original microtechnology makes it possible to carry out classic CMOS electronics on S.O.I wafers but also, in the last stage, and in a way that is self-controlled by the circuit itself, to define the very small interfaces of the Casimir and Coulomb electrodes, the circuit already being encapsulated.

This study thus clarifies the physical limitations of electromechanical systems assisted by the Casimir interaction, while highlighting their potential interest as demonstrators of energy redistribution mechanisms in nanometric devices, rather than as net power generators.

The system, without requiring a conventional external power supply, redistributes its internal configuration energy into usable electrical signal peaks, which are converted into a usable DC voltage without violating the principle of conservation of energy. The repetitive current peaks provided by the RLC circuit appear sufficient to ensure the transformation, in a few milliseconds, of the periodic signal peaks from the passive RLC circuit into a usable DC voltage of several volts.

We observed that in the referential of our 4 dimensions Space-Time plus the Quantic Vacuum, the energy seems to be conserved which is consistent with Noether's theorem.

It is important to reiterate that the system does not extract energy from the quantum vacuum but rather harnesses the mechanical work induced by the Casimir force, converting it into electrical energy through the piezoelectric bridge and synchronized charge commutation. This is described as a preliminary result, as the theoretical aspects summarized here have not yet been examined in full detail:

• **Neglect of Nonlinearity:** The linear dynamic equations do not account for nonlinear electrostatic spring effects or nonlinear material responses, especially at small scales.
• **Idealized Joint and Surface Conditions:** While the assumption of perfectly flat, mirror-like Casimir plates does not hold true at the nanometer scale, the angstrom-level precision provided by ALD—especially in the final stages of assembly—should enable sufficiently consistent and reproducible resolution.
• **Unvalidated Mechanical Model:** I was unable to make any comparison with experimental MEMS resonance data or complete 3D FEM models (e.g., from high-fidelity COMSOL or ANSYS simulations).

Piezoelectric Material Selection

The simulations assume ideal material properties, without accounting for thin-film degradation, surface effects, or substrate interactions.

• PZT : Simulations show feasible behavior with moderate current peak output. However, PZT is lead-based, raising environmental and manufacturing concerns.

• PMN–PT :Shows the highest theoretical performance due to a very high piezoelectric coefficient ($d_{31} \approx 1450$ pC/N). However, film deposition at microscale with preserved d_{31} is technologically nontrivial. The required ~10 µm thick layers are difficult to deposit uniformly while maintaining crystalline orientation and domain structure.

Electrical Conversion Circuit

The energy harvested from the piezo is routed through a MOSFET-controlled switching circuit and then rectified and multiplied using a passive voltage multiplier network. We remark that :

• Efficiency Assumptions: Simulations ignore MOSFET leakage, gate capacitance, threshold variability, and parasitic losses.
• Timing Stability: The concept relies on perfect triggering of MOSFETs based on charge thresholds that are sensitive to temperature and manufacturing variability.
• Lack of Practical Data: No load-line analysis, impedance matching, or power trace simulation is provided.
• No test circuit is presented or fabricated.

Technological Feasibility

The microfabrication scheme (using SOI wafers, etching, sputtering, etc.) is standard in concept, but several issues are overlooked:
• Surface Purity: Any contamination layer (organic films) on Casimir plates suppresses the effect significantly.
• Integration Complexity: Combining PMN–PT films, metal contacts, and active electronics on a single substrate with tight thermal and mechanical tolerances might be complex.
• Switching Timing Precision: The exact timing and response of the electrostatic reset stage relies on transistor thresholds differing by as little as tens of millivolts must be validated .

Physical Realism and Fundamental Objection

• Can vacuum energy actually be extracted? Indeed, within the framework of the dominant quantum field theory, Casimir energy is a potential well, not an energy source.
• Stability of Oscillations: No analysis of long-term stability, phase noise, or stochastic behavior under the influence of vacuum fluctuations has been performed.
• Lack of Empirical Evidence: All claims remain theoretical. I lack the means to build a MEMS prototype for proof-of-concept demonstration to either refute or confirm the conclusions. We believe that, despite the verifications mentioned above, this concept warrants further investigation. The fabrication of a prototype would be the decisive criterion for its confirmation. The theoretical results of this project appear sufficiently encouraging to justify the development of prototypes.

Future Prospects

Several avenues can be explored to advance this work towards experimental realization:
• Fabrication of a MEMS prototype: Using established SOI processes, the central Casimir piezoelectric structure could be fabricated and tested for spontaneous oscillation and charge generation in a vacuum.
• Optimization of the electrostatic tuning mechanism: Improving the design and control of the Coulomb force would allow for precise adjustment of the system's stability point, thus increasing energy production and frequency control.

• Integration with ultra-low threshold CMOS electronics: Coupling the system with high-impedance, low-power electronics would enable the development of autonomous energy harvesting modules for applications in nanometric sensors or space applications.
• Extension to NEMS and 2D material interfaces: Miniaturizing the NEMS architecture and incorporating graphene or MoS_2 layers could significantly improve sensitivity to vacuum forces while reducing friction and energy losses.
• Experimental quantification of energy transfer induced by the Casimir effect. Developing precision instruments to measure the net energy extracted over time would help validate the theoretical model and quantify the practical limitations. This work paves the way for a new generation of autonomous microdevices operating at the interface between classical and quantum physics.
This work was carried out entirely by a retired individual. It seems that, barring any errors, Emmy Noether's fundamental theorem of 1905 remains unchallenged.

If theoretical confirmation is obtained by specialists, the creation of a prototype will constitute the ultimate and definitive assessment. If its theoretical predictions are confirmed, it will lead to significant scientific, technological, and human advancements.
This vacuum energy MEMS concept was carried out by an old retiree , completely alone and without the help of any organization
As the inventor, I would like to collaborate on their development after signing a contract with the potential investor..
"*In the universe, everything is energy, everything is vibration, from the infinitely small to the infinitely large" Albert Einstein.*
"A person who has never made mistakes has never tried to innovate." Albert Einste

References

1. Reynaud, S., Lambrecht, A., Genet, C., Jaekel, M. T. (2001). Fluctuations du vide quantique. Comptes Rendus de l'Academie des Sciences Series IV Physics, 9(2), 1287-1298.
2. Casimir, H. B. (1948). On the attraction between two perfectly conducting plates. In Proc. Kon. Ned. Akad. Wet. (Vol. 51, p. 793).
3. Lambrecht, A., Reynaud, S. (2000). Casimir force between metallic mirrors. The European Physical Journal D, 8(3), 309-318; Lifshitz, E. M., Pitaevskii, L. P., Berestetskii, V. B. (1980). Landau and lifshitz course of theoretical physics. Statistical physics, Part 2 Ch VIII.
4. Deryagin, B. V., Abrikosova, I. I. (1956). Direct measurement of the molecular attraction of solid bodies. 2. Method for measuring the gap. Results of experiments. J. Exp. Theo. Phys., 3, 819-829.
5. Vasic, D., Costa, F. (2011). Applications des éléments piézoélectriques en électronique de puissance. Editions TI.
6. Wachel, J. C., Bates, C. L. (1976). Techniques for Controlling Piping Vibration and Failures. ASME paper, 76-Pet-18.
7. Parasuraman, J., Summanwar, A., Marty, F., Basset, P., Angelescu, D. E., Bourouina, T. (2014). Deep reactive ion etching of sub-micrometer trenches with ultra high aspect ratio. Microelectronic engineering, 113, 35-39.
8. Marty, F., Rousseau, L., Saadany, B., Mercier, B., Français, O., Mita, Y., Bourouina, T. (2005). Advanced etching of silicon based on deep reactive ion etching for silicon high aspect ratio microstructures and three-dimensional micro-and nanostructures. Microelectronics journal, 36(7), 673-677.
9. Sze, S. M. (2008). Semiconductor devices: physics and technology. John wiley & sons.
10. Barthes, M., MECHANICAL, M. C. D. F. S. Vibrational physics. ESTP:(Special School of Public Works).
11. Sangouard, P. (1987). Modélisation de transistors polysilicium en couches minces sur isolants: conception et réalisation d'écrans plats à cristaux liquides et matrices actives (Doctoral dissertation, Paris 11).